**Molecular Therapy**
Original Article

# Antisense oligonucleotide therapy mitigates autosomal dominant progressive hearing loss in a murine model of human DFNA2

Seung Hyun Jang,[1,2,6] Jae Won Roh,[1,2,6] Kyung Seok Oh,[1,2] Sun Young Joo,[1,2] Jung Ah Kim,[1,2] Se Jin Kim,[1,2] Jae Young Choi,[2,3] Jinsei Jung,[2,3] Yeonjoon Kim,[4] Jinwoong Bok,[2,3,5] and Heon Yung Gee[1,2]

[1]Department of Pharmacology, Graduate School of Medical Science, Brain Korea 21 Project, Yonsei University College of Medicine, Seoul, Republic of Korea; [2]Won-Sang Lee Institute for Hearing Loss, Seoul, Republic of Korea; [3]Department of Otorhinolaryngology, Yonsei University College of Medicine, Seoul, Republic of Korea; [4]Qmine, Seoul, Republic of Korea; [5]Department of Anatomy, Brain Korea 21 Project for Medical Science, Yonsei University College of Medicine, Seoul 03722, Republic of Korea

**Hearing loss is the most common sensory disorder, with a substantial proportion caused by genetic mutations. *KCNQ4*, a voltage-gated potassium channel highly expressed in cochlear outer hair cells, is a common genetic etiology implicated in autosomal dominant progressive hearing loss (DFNA2). The dominant-negative *KCNQ4* p.W276S (c.827G>C) mutation represents a mutational hotspot in DFNA2, yet no effective treatments exist. Here, we developed allele-preferential antisense oligonucleotides (ASOs) targeting this dominant-negative *KCNQ4* mutation. In a systemic *in vitro* screen, ASO-123 demonstrated a knockdown of mutant *Kcnq4* while preserving wild-type transcripts. In a *Kcnq4* p.W277S knockin mouse model mimicking DFNA2, ASO-123 preferentially suppressed mutant transcripts, attenuated progressive hearing loss, and improved outer hair cell survival while enhancing their electrophysiologic function. Comprehensive transcriptomic analyses further validated the efficacy of ASO-123. Thus, our findings establish ASO-based therapy as a promising strategy for treating hereditary hearing loss caused by dominant-negative *KCNQ4* mutations.**

## INTRODUCTION

Hearing loss is the most common sensory organ disorder, affecting over 5% of the world's population and incurring an annual global economic cost exceeding $980 billion.[1] Genetic factors contribute substantially to hearing loss, accounting for more than 50% of congenital cases[2] and 30%–40% of post-lingual hearing loss.[3] Despite this burden, there are no approved biological treatments to effectively prevent or reverse genetic hearing loss.

Although more than 150 genes have been implicated in hearing loss, a considerable proportion of hereditary hearing loss cases are linked to mutations in *KCNQ4*, which cause autosomal dominant, non-syndromic hearing loss (DFNA2 [deafness, autosomal dominant 2A]).[4,5] *KCNQ4* encodes a voltage-gated potassium channel (Kv7.4) that is highly expressed on the basolateral surface of cochlear outer hair cells (OHCs), where it mediates potassium efflux critical for OHC repolarization.[6] Biallelic knockout of the *Kcnq4* gene in mice causes progressive, ski-sloping hearing loss with prominent OHC degeneration, highlighting the essential role of *KCNQ4* in maintaining normal hearing.[7] While some deafness-causing *KCNQ4* variants induce hearing loss through gain of function[8] or haploinsufficiency,[9] most variants operate through a dominant-negative effect, wherein the mutant KCNQ4 exerts a deleterious effect on wild-type (WT) KCNQ4.[4,10] This dominant-negative mechanism arises because fully functional KCNQ4 channels are formed by the assembly of tetrameric subunits. Among over 40 pathogenic mutations associated with DFNA2 (Deafness Variation Database: https://deafnessvariationdatabase.org/), the c.827G>C; p.W276S mutation in the *KCNQ4* gene is one of the most frequently reported dominant-negative mutations, representing a mutational hot spot in the *KCNQ4* gene.[10–12] We previously demonstrated that *Kcnq4* p.W277S knockin mice harboring the homologous mutation to human *KCNQ4* p.W276S recapitulate the progressive hearing loss observed in DFNA2 patients, including the predominant degeneration of OHCs.[13]

Recent advances in elucidating the mechanisms underlying genetic hearing loss, along with the development of diverse AAV serotypes and promoter systems, have enabled the successful application of AAV-based gene replacement therapy in several preclinical models and even in human patients.[14–18] However, this gene replacement approach is not effective for hearing loss resulting from dominant-negative or gain-of-function mutations. In addition, although

---

Received 21 January 2025; accepted 28 August 2025;
https://doi.org/10.1016/j.ymthe.2025.08.044.

[6]These authors contributed equally

**Correspondence:** Jinwoong Bok, Department of Anatomy, Brain Korea 21 Project for Medical Science, Yonsei University College of Medicine, Seoul 03722, Republic of Korea.
**E-mail:** bokj@yuhs.ac
**Correspondence:** Heon Yung Gee, Department of Pharmacology, Graduate School of Medical Science, Brain Korea 21 Project, Yonsei University College of Medicine, Seoul, Republic of Korea.
**E-mail:** hygee@yuhs.ac

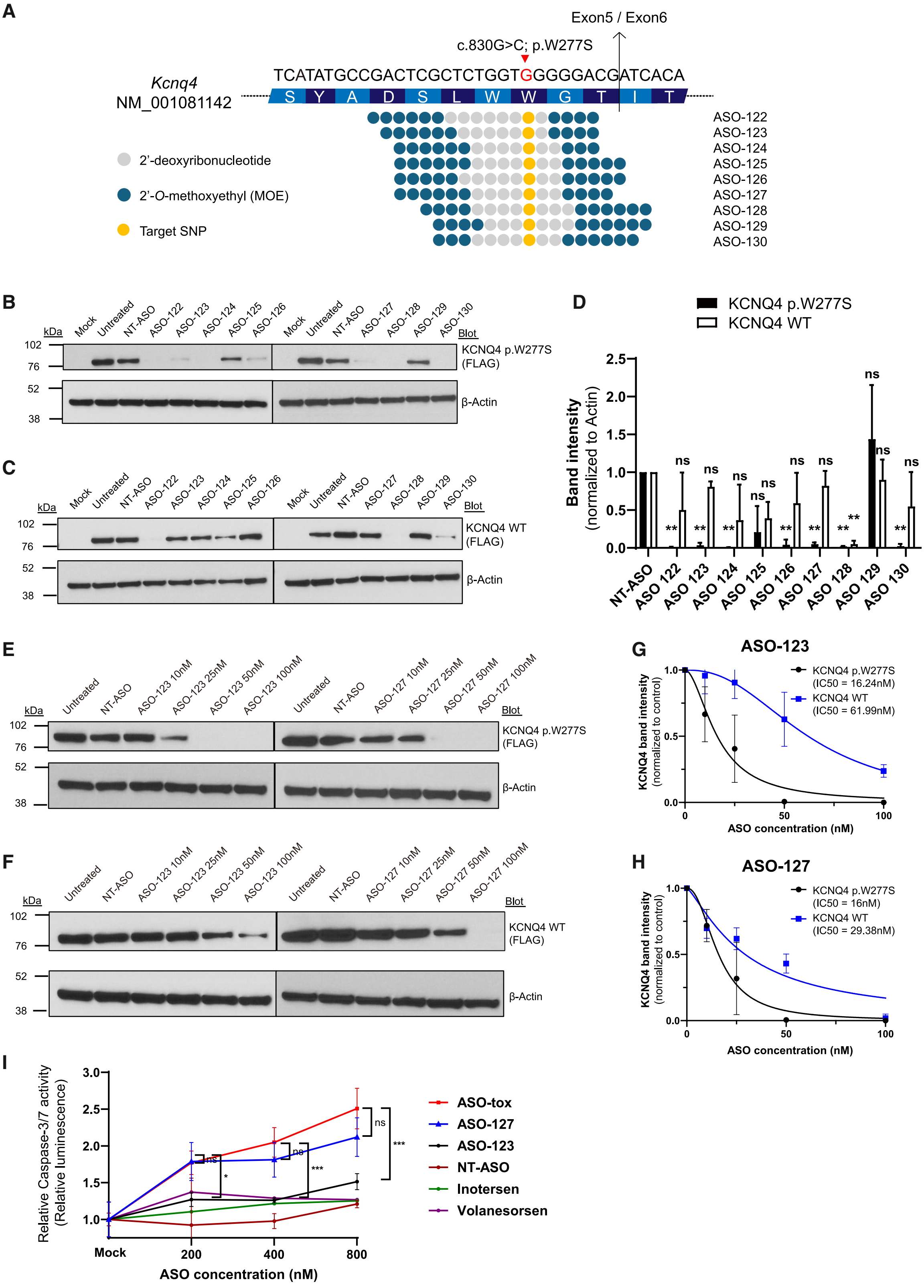

*(legend on next page)*

CRISPR-Cas9-based strategies show promise for these types of mutations,[13,19,20] there are still notable safety concerns with their use. These include off-target mutations,[21,22] the generation of large structural variants, and AAV genome integration at the target sites,[23–25] which can trigger p53-driven DNA damage responses.[26] Additional challenges arise from immune responses to AAV vectors carrying the CRISPR-Cas9 system, which can lead to detrimental morbidities,[27,28] and the neutralizing antibodies against AAV that may compromise therapeutic efficacy and preclude repeated administration.[14,29]

Antisense oligonucleotides (ASOs) present an alternative approach that has been used successfully to treat various neurological disorders by modulating cryptic splicing events[30–32] or by triggering RNase-H1-mediated degradation of mutant alleles.[33–36] ASOs are chemically modified oligonucleotides that offer strong target specificity and minimal toxicity. While splice-switching ASOs are effective for treating Usher syndrome-related hearing loss in mice,[37,38] the therapeutic potential of RNase-H1-dependent gapmer ASOs targeting dominant-negative heterozygous mutations that cause hearing disorders remains unclear.

Here, we developed allele-preferential ASOs targeting a dominant-negative *Kcnq4* mutation and investigated their therapeutic potential in the inner ear using the *Kcnq4* p.W277S mouse model.[13] We demonstrated that preferential knockdown of mutant transcripts significantly ameliorated progressive hearing loss, improved hair cell survival and function, and restored critical biological processes essential for hearing maintenance. Our findings provide a clear proof-of-concept for the development of ASO-based therapies targeting various dominant-negative or gain-of-function mutations associated with hereditary hearing loss, and establish a foundation for future clinical translation.

## RESULTS

### *In vitro* screening of candidate allele-specific ASOs targeting the *Kcnq4* p.W277S mutation

To selectively silence the *Kcnq4* p.W277S mutation, we designed multiple gapmer ASOs, each 16–18 nucleotides (nt) in length, consisting of 7–8 bases of 2′-deoxyribonucleotides in the middle (gap), flanked by 3–6 bases at both the 5′ and 3′ ends (wings) modified at the 2′-O position of ribose with a methoxyethyl (MOE) group. All nucleotides were linked by a phosphorothioate backbone. Based on previous efforts to rationally design allele-specific ASOs through chemical and structural motif modifications,[39,40] we performed a sequence microwalk around the target SNP, while positioning the SNP within the gap, with its length shortened to 7 or 8 nt to ensure specific RNase-H1 cleavage, in conjunction with the varying number of high-affinity MOE-modified nucleotides in the wings (Figure 1A; Table S1). ASOs with this gapmer chemistry elicit knockdown of target transcripts primarily through RNase-H1-mediated degradation.[41] To evaluate the potency and selectivity of the various ASOs, we co-transfected HEK293T cells with *Kcnq4* p.W277S or WT plasmids and one of the candidate ASOs. We then assessed target protein expression levels after a 48-h incubation, as regulation at the protein level is the final endpoint of the treatment. Initial evaluation showed that KCNQ4 protein expression from the p.W277S and WT plasmids were comparable and unaffected by treatment with a non-targeting scrambled ASO (NT-ASO) (Figure S1). Compared with NT-ASO, several ASOs exhibited potent knockdown efficacy against the *Kcnq4* p.W277S mutation (Figure 1B), while some also displayed high selectivity against the WT *Kcnq4* (Figure 1C). To statistically evaluate the allelic discrimination capacity of each ASO, we used two-way analysis of variance (ANOVA) to compare the impact of the various ASOs on the expression from each target relative to NT-ASO treatment (Figure 1D). This analysis, conducted at a screening concentration of 50 nM, allowed us to identify two ASOs (ASO-123 and -127) that significantly suppressed mutant KCNQ4 while preserving WT expression, and that led to the most pronounced differences in expression levels between the two targets.

To characterize and compare the dose-dependent potency and selectivity of these two promising ASOs (ASO-123 and -127), we measured target protein expression in cells treated with varying concentrations of each ASO (Figures 1E–1H). Both ASO-123 and -127 inhibited the expression of mutant KCNQ4 protein in a dose-dependent manner, exhibiting similar potency (half-maximal inhibitory concentrations [$IC_{50}$] for ASO-123: 16.24 nM; $IC_{50}$ for ASO-127: 16 nM). These potencies are comparable with those of ASOs previously approved for clinical use.[30] In terms of selectivity, ASO-123 showed better results than ASO-127, with an $IC_{50}$ of 61.99 nM compared with 29.38 nM for ASO-127. We calculated the $IC_{50}$ ratio for the effects of ASO-123 and -127 on the KCNQ4 WT and W277S proteins as another marker for allelic discrimination and found that ASO-123 showed a 2.08-fold greater selectivity than ASO-127 ($IC_{50}$ for WT/$IC_{50}$ for W277S; ASO-123: 3.82; ASO-127: 1.84). We also confirmed the effects of ASO-123 and -127 at the mRNA level

**Figure 1. *In vitro* screening of candidate ASOs**

(A) Schematic alignment of nine candidate allele-specific gapmer ASOs targeting the *Kcnq4* p.W277S mutation. The full sequences and chemical modifications of these ASOs are presented in Table S1. (B and C) Representative western blot images assessing the potency (B) and selectivity (C) of the nine candidate ASOs (50 nM). NT-ASO indicates NT-ASO1 in Table S1. (D) KCNQ4 p.W277S or WT protein band intensities were normalized to β-actin and then to NT-ASO-treated controls ($n = 3$ per treatment). Data are shown as mean ± SD. Statistical significance was determined via two-way ANOVA with Bonferroni's corrections for multiple comparisons. ns, not significant; $^{**}p < 0.01$. (E and F) Representative western blot images showing KCNQ4 p.W277S (E) or WT (F) levels following treatment with NT-ASO (100 nM) or various concentrations of ASO-123 or -127. NT-ASO indicates NT-ASO1 in Table S1. (G and H) Dose-response curves of ASO-123 (G) and ASO-127 (H) for KCNQ4 p.W277S or WT, normalized to β-actin and then to untreated controls. Data are presented as mean ± SD ($n = 3$). (I) Relative caspase-3/7 activity in HeLa cells, normalized to mock-treated samples 8 h after ASO transfection. Data are shown as mean ± SD ($n = 3$). Statistical significance was determined via two-way ANOVA with Dunnett's corrections for multiple comparisons. ns, not significant; $^{*}p < 0.05$, $^{**}p < 0.01$, $^{***}p < 0.001$.

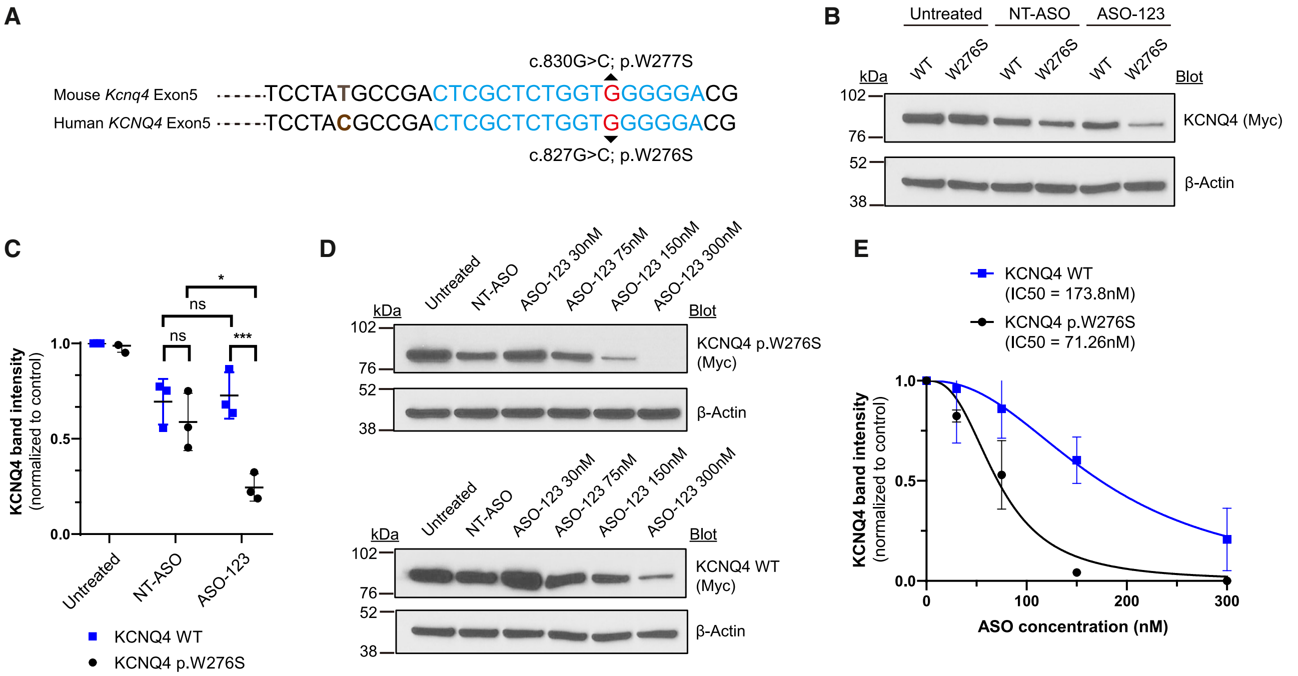

**Figure 2. ASO-123 shows allelic preference for human KCNQ4 p.W276S over KCNQ4 WT**

(A) Alignment of the regions of the human *KCNQ4* and mouse *Kcnq4* exon5 sequences surrounding the target mutation (c.827G>C; p.W276S in human *KCNQ4*). The ASO-123 target sequence and target mutation are highlighted in sky-blue and red, respectively, with the mismatched base shown in brown. (B) Representative western blot images showing KCNQ4 WT or W276S bands following treatment with NT-ASO or ASO-123 (150 nM). (C) KCNQ4 WT and W276S protein band intensities normalized first to β-actin and then to the untreated KCNQ4 WT intensities. Data are presented as mean ± SD ($n = 3$). Statistical significance was determined via two-way ANOVA with Tukey's corrections for multiple comparisons. ns, not significant; $^{*}p < 0.05$, $^{**}p < 0.01$, $^{***}p < 0.001$. NT-ASO indicates NT-ASO2 in Table S1. (D) Representative western blot images showing KCNQ4 WT or W276S bands after treatment with NT-ASO or ASO-123 across a range of concentrations (30–300 nM). (E) ASO-123 dose-response curves for KCNQ4 W276S and WT band intensities normalized to β-actin and then to untreated controls. Data are presented as mean ± SD ($n = 3$).

recapitulated our findings at the protein level (Figure S2). Collectively, these results suggest ASO-123 potently and preferentially reduces KCNQ4 p.W277S protein expression with approximately 3.82-fold higher affinity for the mutant allele over the WT allele *in vitro*.

Since ASOs with phosphorothioate bonds can elicit toxicity via caspase-mediated apoptosis,[42] we transfected HeLa cells with ASO-123, -127, NT-ASO, a known toxic ASO (ASO-tox),[42] or two FDA-approved gapmer ASOs (inotersen[43] and volanesorsen[44]) at various concentrations and assessed caspase-3/7 activation to evaluate potential safety concerns for *in vivo* experiments (Figure 1I). Consistent with a previous report, we observed approximately 2.5-fold more caspase-3/7 activation in samples treated with 800 nM ASO-tox than in mock-treated controls. Notably, ASO-127 and ASO-tox induced similar levels of caspase activation. In contrast, ASO-123 induced significantly less caspase-3/7 activation than ASO-tox, even at 800 nM—a concentration 49.26 times higher than the $IC_{50}$ of ASO-123 for KCNQ4 p.W277S *in vitro*. Furthermore, we found similar caspase-3/7 activation levels induced by ASO-123 and the FDA-approved ASOs. Finally, we examined the off-target profile of ASO-123. We searched for genomic regions containing a single internal nucleotide mismatch or indel relative to the full-length ASO sequence, as well as perfect matches to 5′ end- or 3′ end-trimmed subsequences, all of which may represent biologically meaningful off-targets.[45] This analysis revealed that ASO-123 has a comparable, or even cleaner, off-target profile in the mouse genome than other FDA-approved ASOs (nusinersen,[46] splice-switching ASO; inotersen,[43] gapmer ASO; Tables S2–S4). Together, these results suggest a safer profile for ASO-123 than ASO-127.

### ASO-123 exhibits allelic preference for human *KCNQ4* p.W276S over *KCNQ4* WT

Since the region of mouse *Kcnq4* exon5 surrounding the target mutation (*Kcnq4* c.830G>C; p.W277S, homologous to human *KCNQ4* c.827G>C; p.W276S) and the ASO-123 target sequence are highly conserved between human and mouse (Figure 2A), we next asked whether ASO-123 exhibits a similar allelic preference for the human *KCNQ4* p.W276S mutation over *KCNQ4* WT, resembling that in mouse *Kcnq4*. To answer this question, we co-transfected HEK293T cells with either *KCNQ4* WT or W276S, treated them with either NT-ASO or ASO-123 (both at 150 nM), and then measured protein expression 48 h post-transfection. We found that, compared with NT-ASO-treated samples, ASO-123 significantly reduced KCNQ4 W276S expression, while preserving KCNQ4 WT expression (Figures 2B and 2C). In a further

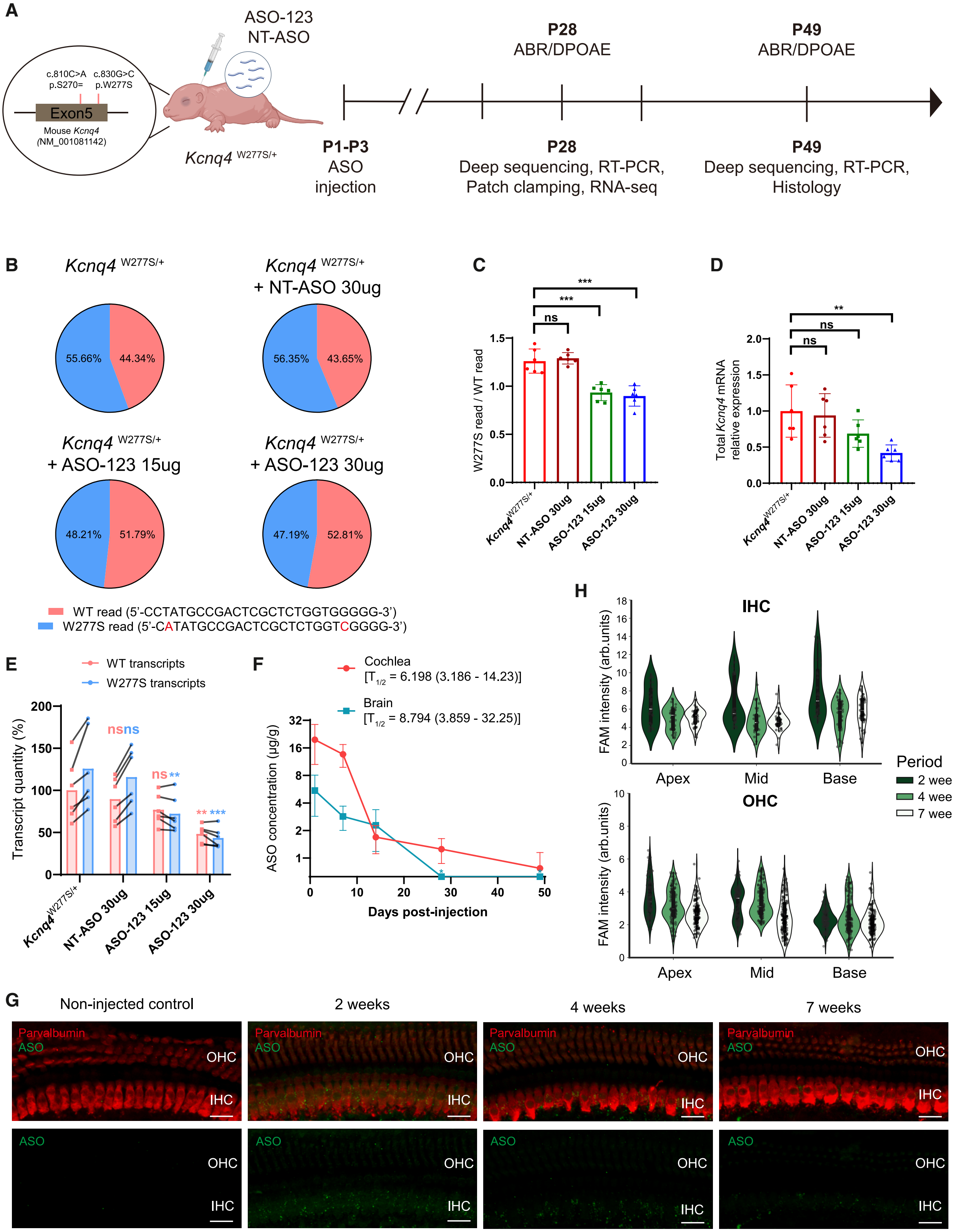

*(legend on next page)*

dose-response analysis, the $IC_{50}$ values indicated a pronounced preferential knockdown of KCNQ4 W276S over KCNQ4 WT ($IC_{50}$ for KCNQ4 W276S: 71.26 nM; $IC_{50}$ for KCNQ4 WT: 173.8 nM) (Figures 2D and 2E). At the mRNA level, this trend was replicated, albeit more sensitively than at the protein level (Figure S3), which was consistent with previous findings.[34] Together, these findings indicate that ASO-123 shows strong allelic preference for human *KCNQ4* W276S over *KCNQ4* WT and highlight its potential as a targeted therapeutic approach for human DFNA2 caused by the *KCNQ4* c.827G>C mutation.

### *In vivo* delivery of ASO-123 preferentially knocks down mutant *Kcnq4* transcripts over WT transcripts

We selected ASO-123 as the final candidate for *in vivo* validation owing to its potency, selectivity, safety (Figure 1), and dual-targeting potential for both human *KCNQ4* p.W276S and mouse *Kcnq4* p.W277S mutations (Figure 2). First, to assess the transfection efficiency of locally delivered ASO in hair cells, we injected WT mice through the round window membrane (RWM) with fluorescein-NT-ASO (FAM-NT-ASO) on postnatal days 1–3 (P1–P3). Four weeks post-injection, we observed fluorescein-ASO in nearly all inner hair cells (IHCs) and most OHCs, with an increasing gradient from the apex to the base of the cochlea (Figure S4), consistent with a previous report.[37] Furthermore, we also found that ASOs delivered via the RWM were distributed to other regions of the cochlea, including the stria vascularis, spiral ligament, spiral limbus, spiral ganglion neurons (SGNs), and even to multiple regions of the brain, probably via the cochlear aqueduct[47] (Figure S5). These data demonstrate a broad biodistribution of ASOs locally delivered to the inner ear.

Next, to evaluate the *in vivo* efficacy of ASO-123 against the *Kcnq4* p.W277S mutation, we injected *Kcnq4* p.W277S heterozygous mice (hereafter, $Kcnq4^{W277S/+}$) at P1–P3 through the RWM with either 15 or 30 μg of ASO-123 and 30 μg of NT-ASO as a control (Figure 3A). The initial dosage was based on a previous study that assessed the therapeutic potential of a splice-switching ASO for type I Usher syndrome in the inner ear using a delivery approach similar to that used in this study.[37] Because there is only a single nucleotide difference separating the *Kcnq4* WT and W277S transcripts, we were unable to identify any primers that could specifically and reliably amplify only the *Kcnq4* W277S transcript. Additionally, neither could we find an antibody to distinguish the KCNQ4 W277S and WT proteins by western blot or immunofluorescence staining. However, the *Kcnq4* W277S allele in our mouse model does harbor an additional synonymous mutation (c.810C>A; p.S270=) upstream of the target mutation (c.830G>C; p.W277S) that enables selective cleavage of the W277S allele and not the WT allele by the NdeI restriction enzyme (Figure S6A). Leveraging this feature, we initially performed a semi-quantitative restriction fragment-length polymorphism (RFLP) analysis using cochlear cDNA from injected and non-injected $Kcnq4^{W277S/+}$ mice at P28, a time by which *Kcnq4* expression should have reached their mature levels throughout the cochlear turns (approximately P21–P23).[48] In this RFLP analysis, we observed a significant reduction of the bands corresponding to the W277S allele for mice treated with 15 or 30 μg of ASO-123, compared with those of untreated mice. Although the band intensities for the WT allele remained similar in the ASO-123 15 μg-treated group, they showed a tendency to decrease in mice injected with 30 μg of ASO-123 (Figures S6B–S6C). To more precisely evaluate allele-specific expression changes following ASO-123 treatment, we conducted targeted deep sequencing of *Kcnq4* transcripts using cDNA from the injected and non-injected cochleae of $Kcnq4^{W277S/+}$ mice at age 4 weeks and compared the proportions of WT and W277S transcripts. Non-injected cochleae and cochleae injected with NT-ASO produced 55.66% ± 2.41% (mean ± SD, non-injected) and 56.35% ± 1.16% (NT-ASO) W277S transcripts, respectively. In contrast, cochleae injected with either 15 or 30 μg of ASO-123

**Figure 3. *In vivo* efficiency of ASO-123 administration in the inner ear**

(A) Schematic timeline of the *in vivo* experiments. $Kcnq4^{W277S/+}$ mice harbor the *Kcnq4* c.830G>C (p.W277S) mutation, which is homologous to the human *KCNQ4* c.827G>C (p.W276S) mutation. They also harbor the c.810C>A (p.S270=) synonymous mutation to facilitate genotyping by restriction fragment-length polymorphism (RFLP). (B) Pie charts displaying the proportion of WT and W277S reads among *Kcnq4* transcripts. W277S reads were identified based on the dual presence of the p.W277S mutation (c.830G>C) and the upstream synonymous mutation (c.810C>A). (C) The ratio of W277S to WT read counts across the four groups. Data are presented as mean ± SD ($n = 6$ per group). Statistical significance was determined via one-way ANOVA with Dunnett's corrections for multiple comparisons. ns, not significant; $^{*}p < 0.05$, $^{**}p < 0.01$, $^{***}p < 0.001$. NT-ASO indicates NT-ASO1 in Table S1. (D) RT-PCR results showing total *Kcnq4* expression levels across the four groups. Expression levels were normalized to the *Actb* housekeeping gene and to non-injected samples. Data are presented as mean ± SD ($n = 6$ per group). Statistical significance was determined via one-way ANOVA with Dunnett's corrections for multiple comparisons. ns, not significant; $^{*}p < 0.05$, $^{**}p < 0.01$, $^{***}p < 0.001$. NT-ASO indicates NT-ASO1 in Table S1. (E) Quantification of the WT and W277S transcripts across the four groups. Allele-specific transcript quantities were calculated by combining total *Kcnq4* mRNA levels as determined by RT-PCR (and normalized to the *Actb* housekeeping gene) with the proportion of WT and W277S transcripts as determined by deep sequencing from the same animal. Each allele-specific quantity was then normalized to the average WT transcript level in non-injected samples (set to 100%). Data are presented as means with individual values ($n = 6$ per group). The values from the same mouse are connected by black lines. Statistical significance was assessed using two-way ANOVA with Dunnett's corrections for multiple comparisons. The indicated $p$ values represent comparisons between treated and untreated groups for each allele. ns, not significant; $^{*}p < 0.05$, $^{**}p < 0.01$, $^{***}p < 0.001$. (F) ASO-123 concentration (μg of ASO per gram of tissue) in the cochlea and brain following RWM injection at P1–P3. Data are presented as mean ± SD (1 day post-injection, $n = 2$; 7 days, $n = 3$; 14 days, $n = 3$; 28 days, $n = 3$; 49 days, $n = 3$). The ASO half-life was calculated using non-linear regression and is reported as $T_{1/2}$ (with a 95% confidence interval in days). *Not detected (<0.098 nM). (G) Representative confocal images of parvalbumin (red) and FAM (green) staining in mid-turn (16–18-kHz region) cochleae from untreated $Kcnq4^{+/+}$ and FAM-ASO-123-treated $Kcnq4^{+/+}$ mice at age 2, 4, and 7 weeks. Scale bars, 20 μm. IHC, inner hair cell; OHC, outer hair cell. (H) Violin plots of FAM fluorescence intensity across three time points in individual IHCs and OHCs. Intensities were measured within a 100-μm region of the apical (6–8 kHz), middle (16–18 kHz), and basal (32–34 kHz) turns at age 2, 4, and 7 weeks in FAM-ASO-123 treated $Kcnq4^{+/+}$ mice ($n = 3$ biological replicates per time point). Individual values are shown as black semi-transparent dots.

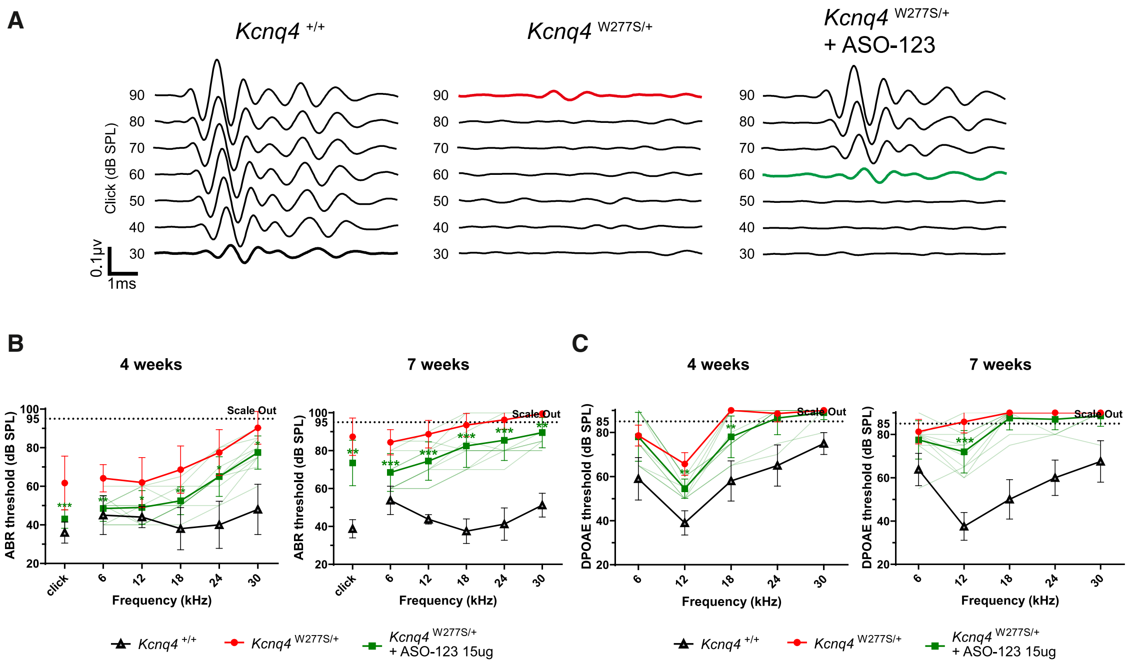

**Figure 4. *In vivo* ASO-123 delivery alleviates the progressive hearing loss of *Kcnq4*$^{W277S/+}$ mice**

(A) Representative ABR waveforms stimulated by broadband click stimuli in WT (*Kcnq4*$^{+/+}$), non-injected *Kcnq4*$^{W277S/+}$, and ASO-123-injected *Kcnq4*$^{W277S/+}$ mice at age 7 weeks. Black, red, and green bold traces indicate thresholds in each group. (B) Average click and tone ABR thresholds at age 4 (left) or 7 (right) weeks in WT, non-injected *Kcnq4*$^{W277S/+}$, and ASO-123-injected *Kcnq4*$^{W277S/+}$ mice (4 weeks: WT, *n* = 5; non-injected *Kcnq4*$^{W277S/+}$, *n* = 9; ASO-123-injected *Kcnq4*$^{W277S/+}$, *n* = 10; 7 weeks: WT, *n* = 4; non-injected *Kcnq4*$^{W277S/+}$, *n* = 16; ASO-123-injected *Kcnq4*$^{W277S/+}$, *n* = 10). Transparent green lines represent thresholds from individual ASO-123-injected *Kcnq4*$^{W277S/+}$ mice. Data are shown as mean ± SD. Statistically significant differences in tone thresholds were assessed via two-way ANOVA with Bonferroni's corrections for multiple comparisons. Differences in click thresholds were assessed via one-way ANOVA with Bonferroni's corrections for multiple comparisons. $^{*}p < 0.05$, $^{**}p < 0.01$, $^{***}p < 0.001$. (C) Average DPOA thresholds at 4 (left) or 7 (right) weeks in WT, non-injected *Kcnq4*$^{W277S/+}$, and ASO-123-injected *Kcnq4*$^{W277S/+}$ mice (4 weeks: WT, *n* = 5; non-injected *Kcnq4*$^{W277S/+}$, *n* = 7; ASO-123-injected *Kcnq4*$^{W277S/+}$, *n* = 10; 7 weeks: WT, *n* = 4; non-injected *Kcnq4*$^{W277S/+}$, *n* = 9; ASO-123-injected *Kcnq4*$^{W277S/+}$, *n* = 10). Transparent green lines represent thresholds from individual ASO-123-injected *Kcnq4*$^{W277S/+}$ mice. Data are shown as mean ± SD. Statistical significance was determined via two-way ANOVA with Bonferroni's corrections for multiple comparisons. $^{*}p < 0.05$, $^{**}p < 0.01$, $^{***}p < 0.001$.

produced fewer W277S transcripts at 48.21% ± 2.25% or 47.19% ± 3.06%, respectively (Figure 3B). We further found that, compared with non-injected cochleae, the ratio of W277S and WT read counts in cochleae injected with 15 or 30 μg of ASO-123 significantly decreased by 25.95% and 28.73%, respectively (Figure 3C). We also evaluated the effect of ASO treatment on total *Kcnq4* mRNA expression level, including both W277S and WT transcripts. Using RT-PCR, we found that while neither NT-ASO nor 15 μg of ASO-123 significantly reduced total *Kcnq4* levels, a higher dose of ASO-123 (30 μg) significantly reduced total *Kcnq4* levels by 58.14% ± 4.58% (Figure 3D). To estimate the allele-specific quantities of W277S vs. WT transcripts in each animal, we multiplied the total *Kcnq4* levels as measured via RT-PCR by the transcript proportions obtained via deep sequencing from the same animal (Figure 3E). This revealed a significant reduction of W277S transcript levels by 42.53% or 65.46% following injection of 15 or 30 μg ASO-123, respectively. In contrast, although WT transcript levels were significantly reduced by 51.81% in the ASO-123 30-μg group compared with untreated mice, there was no significant change in the ASO-123 15-μg group. Together, these results indicate that *in vivo* injections of 15 μg of ASO-123 into the inner ear produced a preferential reduction in *Kcnq4* W277S transcripts over WT transcripts at P28.

To assess time-dependent changes in *Kcnq4* allele expression following ASO-123 administration to the inner ear, we performed RT-PCR to measure total *Kcnq4* mRNA levels and conducted deep sequencing to determine transcript proportions at P49 in *Kcnq4*$^{W277S/+}$ mice injected with 15 μg of NT-ASO or ASO-123 between P1 and P3. First, we compared baseline *Kcnq4* mRNA expression in the cochlea between P28 and P49 in untreated *Kcnq4*$^{W277S/+}$ mice and found similar expression levels at both time points (Figure S7A). Our allele-specific quantification revealed that injection of 15 μg ASO-123 significantly reduced expression of the W277S allele by 46.47% by P49, although with substantial inter-individual variability (Figures S7B–S7D). These findings suggest, at least in some animals, that a single neonatal injection of ASO-123 can preferentially suppress expression of the W277S allele for up to 7 weeks.

To elucidate the pharmacokinetic properties of ASO-123 delivered via the RWM, we performed a hybridization ELISA using cochleae

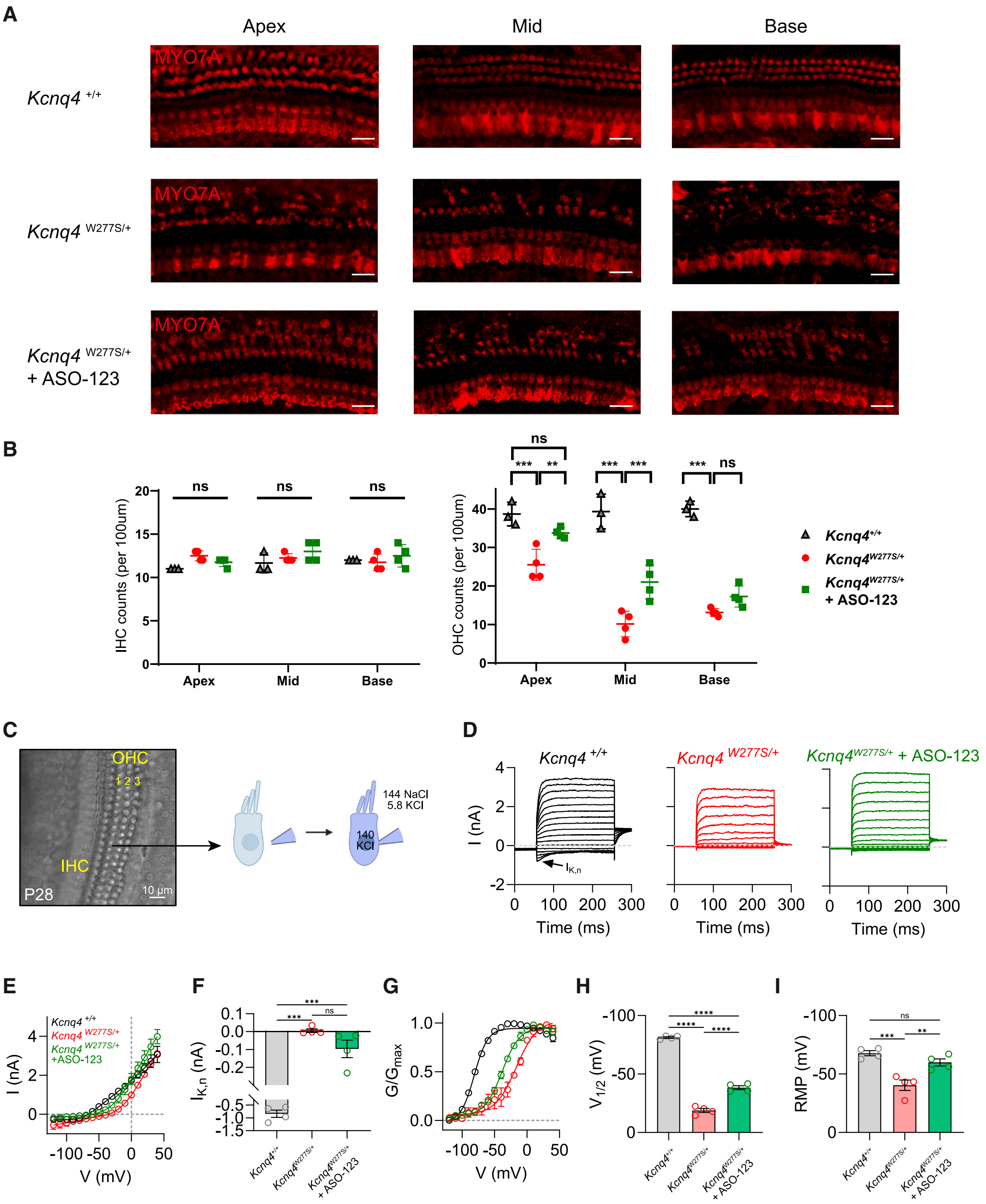

**Figure 5. ASO-123 delivery improves OHC survival and function in *Kcnq4*$^{W277S/+}$ mice**

(A) Representative confocal images of MYO7A staining in whole-mount cochleae from *Kcnq4*$^{+/+}$, untreated *Kcnq4*$^{W277S/+}$, and ASO-123-treated *Kcnq4*$^{W277S/+}$ mice at age 7 weeks. Scale bars, 20 μm. (B) Number of IHCs (left) and OHCs (right) across three cochlear turns in the three groups ($n = 3$–4 per group). Data are presented as mean ± SD. Statistical significance was determined via two-way ANOVA with Bonferroni's corrections for multiple comparisons. ns, not significant; $^{*}p < 0.05$, $^{**}p < 0.01$, $^{***}p < 0.001$. (C) Representative image of a dissected organ of Corti in which KCNQ4 currents were measured at age 4 weeks. (D) Representative current traces from voltage-gated $K^+$ channels in OHCs. The characteristic $I_{K,n}$ that appears in WT OHCs is absent in *Kcnq4*$^{W277S/+}$ OHCs and partially recovered in ASO-123-treated *Kcnq4*$^{W277S/+}$ OHCs. Currents were evoked by 200-ms test pulses at −120 to 40 mV and by a 100-ms post-pulse at −40 mV. (E) Current-voltage relationships for the $K^+$ currents. The current

*(legend continued on next page)*

and ipsilateral brain hemispheres collected at 1, 7, 14, 28, and 49 days post-injection from WT mice that had received 15 μg of ASO-123 at P1–P3 (Figure 3F). We found a rapid decline in ASO concentrations in the cochlea during the first 2 weeks, followed by a more modest decrease thereafter, which gave an estimated half-life of 6.198 days (95% confidence interval [CI], 3.186–14.23 days). Notably, we found that ASO-123 remained detectable in the inner ear for up to 49 days post-injection. In the brain, we were able to detect ASO-123 delivered via RWM injection until 14 days post-injection at concentrations comparable with those in the cochlea, but this disappeared from 28 days onward. Thus, we estimated the half-life of ASO-123 in the brain to be 8.794 days (95% CI, 3.859–32.25 days). To further assess ASO localization in target cells, we performed immunofluorescent staining of the organ of Corti from WT mice injected with 15 μg of 5′-fluorescein-labeled ASO-123 (FAM-ASO-123) via the RWM at P1–P3 (Figure 3G). This allowed us to confirm efficient delivery to the OHCs at 2 weeks that remained up to 7 weeks post-injection (Figure 3H).

To further evaluate the potential ototoxicity of ASO-123 *in vivo*, we injected ASO-123 into WT mice (*Kcnq4*$^{+/+}$) with the same genetic background (C57BL/6N) as *Kcnq4*$^{\mathrm{W277S/+}}$ mice and examined auditory function using the auditory brainstem response (ABR) test at age 4 weeks. Since we could not detect any changes in the ABR thresholds to click or tone stimuli at any frequency in mice injected with either 15 or 30 μg of ASO-123 compared with non-injected mice or mice injected with NT-ASO (Figure S8A), we concluded that the ASO-123 injections did not induce appreciable hearing loss. We next measured the 7-day survival of ASO-injected *Kcnq4*$^{\mathrm{W277S/+}}$ pups following injection at P1–P3 (Figure S8B). Unexpectedly, although pups subjected to the 15 μg ASO-123 and 30 μg NT-ASO injections exhibited comparable survival rates with non-injected pups, the 30 μg ASO-123 injections significantly reduced survival. We did not detect any other notable abnormalities in the mice injected with 15 μg of ASO-123 throughout the 7-week study period, up to P49. As ASOs delivered through the RWM can distribute to the central nervous system via the cochlear aqueduct (Figures S5B and 3F), by scaling cerebrospinal fluid volumes between humans and mice (adult mouse: human ≈ 1:3,000–4,000),[49–51] we estimate that a 30-μg dose in neonatal mice would be equivalent to a dose of 90–120 mg in humans. This may approach or exceed the upper end of the generally well-tolerated range (typically 10–120 mg) reported for intrathecally delivered 2′-MOE gapmer ASOs in humans.[36] While the exact mechanism by which the 30 μg ASO-123 injections reduced viability remains unclear, we concluded that this dose both exceeded the maximal tolerable level and exhibited impaired allelic preference for *Kcnq4* W277S. Thus, we used only the 15-μg dose in subsequent phenotypic evaluations.

### ASO-123 injection ameliorates progressive hearing loss in *Kcnq4*$^{\mathrm{W277S/+}}$ mice

We injected *Kcnq4*$^{\mathrm{W277S/+}}$ mice at P1–P3 with 15 μg of ASO-123 via the RWM and then serially evaluated their ABR thresholds to click and tone stimuli at frequencies ranging from 6 to 30 kHz at 4 and 7 weeks (Figures 4A and 4B). By 7 weeks, non-injected *Kcnq4*$^{\mathrm{W277S/+}}$ mice exhibited severe hearing loss, with no discernible response to mid- to high-frequency stimuli (18–30 kHz) of up to 90 dB SPL. ASO-123-injected *Kcnq4*$^{\mathrm{W277S/+}}$ mice, in contrast, showed a significant reduction in the ABR thresholds across all tested frequencies, including click stimuli, with improvements ranging from 12.5 to 18.67 dB SPL at 4 weeks. At 7 weeks, we observed a significant deceleration of the expected progressive hearing loss with 10.06–15.91 dB SPL improvements in the ABR thresholds to all click and tone stimuli. We next compared the wave I (P1) amplitude and latency stimulated by click, and 6- and 12-kHz tone stimuli at 90 dB SPL in 3 groups of mice at 7 weeks, with 9 of 16 untreated *Kcnq4*$^{\mathrm{W277S/+}}$ mice excluded from the analysis because they showed no discernible waves at 90 dB SPL. This comparison revealed a significant increase in wave I amplitudes of ASO-123-treated *Kcnq4*$^{\mathrm{W277S/+}}$ mice in response to click stimuli compared with untreated *Kcnq4*$^{\mathrm{W277S/+}}$ mice, such that they were even comparable with those of WT mice. Moreover, the wave I amplitudes of ASO-123-treated mice in response to 6- and 12-kHz tone stimuli also showed an increasing trend when compared with those of untreated mice (Figure S9A), and the wave I latency of ASO-123-treated mice showed a decreasing trend compared with that of non-injected *Kcnq4*$^{\mathrm{W277S/+}}$ mice (Figure S9B).

Since KCNQ4 plays a crucial role in the function of OHCs, we also conducted distortion product otoacoustic emission (DPOAE) tests, which more specifically reflect OHC function than ABR tests (Figure 4C). We found an 11.21-dB SPL improvement in the DPOAE threshold in response to a 12-kHz stimulus and a 12-dB SPL improvement in the response to an 18-kHz stimulus at 4 weeks. The significant improvement in the 12-kHz threshold even persisted until 7 weeks. To verify that this alleviation of the progressive hearing loss of *Kcnq4*$^{\mathrm{W277S/+}}$ mice was mediated by an on-target effect of ASO-123, we also evaluated the auditory phenotypes of *Kcnq4*$^{\mathrm{W277S/+}}$ mice injected with NT-ASO (30 μg) at the same time points (P1–P3). We found that NT-ASO injection did not improve ABR or DPOAE results at 4 or 7 weeks, indicating no rescue of hearing loss (Figure S10). Together, these results confirm that the preferential on-target knockdown of *Kcnq4* W277S transcripts by ASO-123 led to an amelioration of the progressive hearing loss of *Kcnq4*$^{\mathrm{W277S/+}}$ mice.

amplitude was analyzed at the 150 ms point during the test pulse. (F) Quantification of $I_{K,n}$ amplitudes ($n = 4$ per group). The current amplitude was analyzed at the 20 ms point during the test pulse at −120 mV. (G) Conductance-voltage relationships for the $K^+$ currents. Conductance was measured by analyzing tail current amplitudes. (H) Half-maximal activation voltage ($V_{1/2}$). Curves were fitted to the Boltzmann equation ($n = 4$ per group). (I) Comparison of OHC resting membrane potentials (RMPs). Data are presented as mean ± SD ($n = 4$ per group). Statistical significance was assessed via one-way ANOVA with Bonferroni's corrections for multiple comparisons. ns, not significant; *$p < 0.05$, **$p < 0.01$, ***$p < 0.001$.

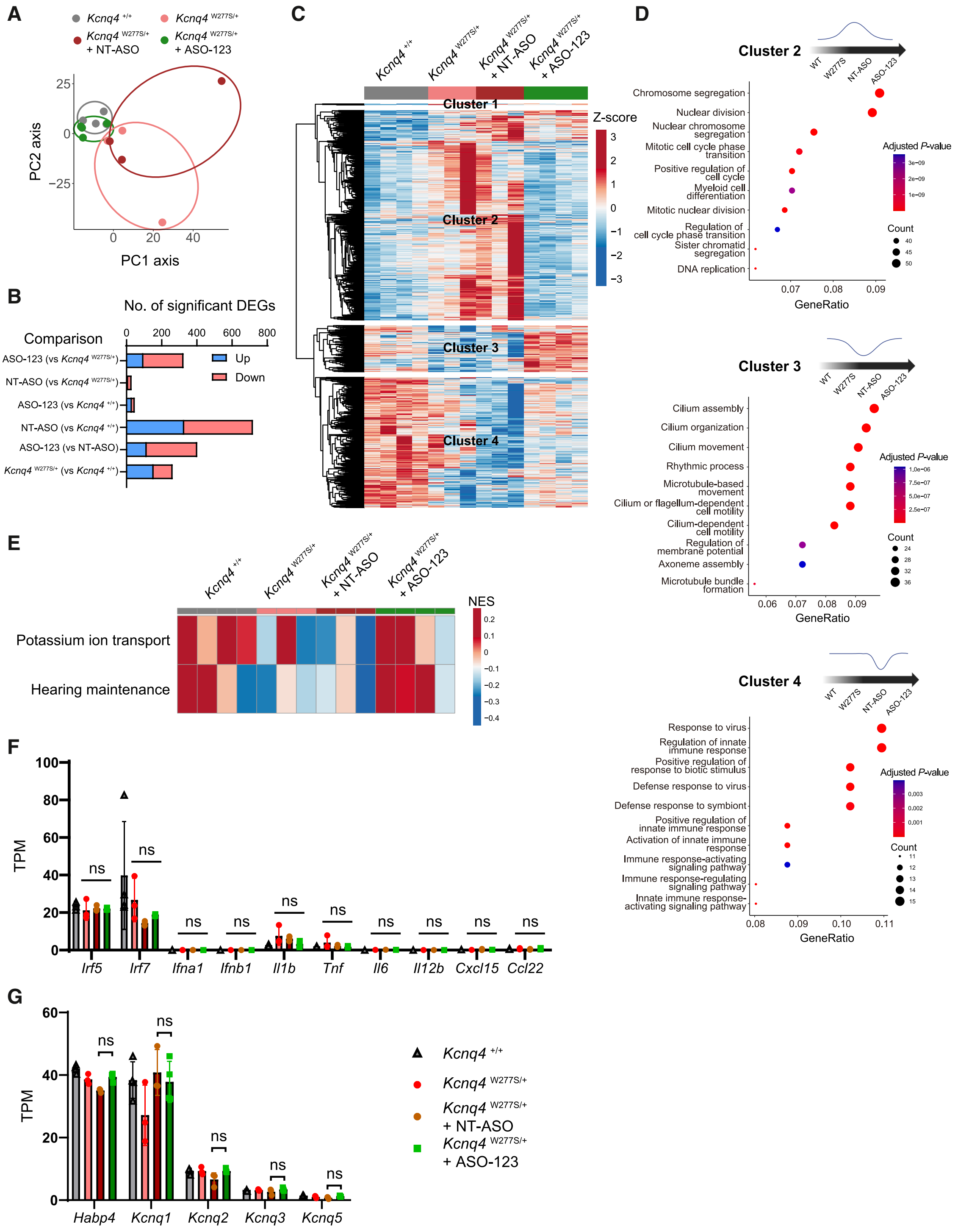

**Figure 6. Transcriptomic alterations following ASO treatment in *Kcnq4*$^{W277S/+}$ mice**

(A) Principal-component analysis (PCA) plot of RNA sequencing data from the four groups (*Kcnq4*$^{+/+}$, *Kcnq4*$^{W277S/+}$, *Kcnq4*$^{W277S/+}$ + NT-ASO 15 μg, and *Kcnq4*$^{W277S/+}$ + ASO-123 15 μg) ($n = 3$–4 per group). NT-ASO indicates NT-ASO1 in Table S1. (B) Bar plot showing the number of significant differentially expressed genes (DEGs) (Benjamini-Hochberg-adjusted $p < 0.05$) between the indicated groups. NT-ASO, *Kcnq4*$^{W277S/+}$ + NT-ASO 15 μg; ASO-123, *Kcnq4*$^{W277S/+}$ + ASO-123 15 μg. (C) Heatmap of Z-scored, normalized expression levels for the significant DEGs (Benjamini-Hochberg-adjusted $p < 0.05$) across all comparisons. Hierarchical clustering was performed to identify DEG clusters. (D) The 10 most significantly enriched Gene Ontology (GO) terms (Benjamini-Hochberg-adjusted $p < 0.05$) for each DEG cluster, as ranked according to gene ratio

*(legend continued on next page)*

### ASO-123 delivery into the inner ear of *Kcnq4*$^{W277S/+}$ mice promotes OHC survival and function

We and others previously demonstrated that hearing loss of mice harboring dominant-negative *Kcnq4* mutations is primarily due to the degeneration of OHCs, without prominent deterioration of IHCs or SGNs.[7,13,52,53] Since ASO-123 prevented hearing loss in *Kcnq4*$^{W277S/+}$ mice, we used the hair cell marker MYO7A to evaluate OHC survival in 7-week-old *Kcnq4*$^{W277S/+}$ mice injected with 15 μg of ASO-123 (Figures 5A and 5B). As expected, untreated *Kcnq4*$^{W277S/+}$ mice showed marked OHC degeneration at 7 weeks, particularly in the mid and basal turns of the cochlea. We did not observe any significant differences in the number of IHCs between WT and *Kcnq4*$^{W277S/+}$ mice. In *Kcnq4*$^{W277S/+}$ mice injected with ASO-123, we observed a significant increase in OHC survival in the apical and mid-turns compared with untreated *Kcnq4*$^{W277S/+}$ mice. The limited improvement in OHC survival in the basal turn may explain the minimal enhancement of high-frequency DPOAE thresholds at 7 weeks. Additionally, we did not find any significant changes in the number of surviving SGNs in Rosenthal's canal or neurofilaments from type II SGNs innervating the OHCs in any of the three cochlear turns across any of the three groups, indicating that SGN degeneration did not occur substantially up to P49 in *Kcnq4*$^{W277S/+}$ mice (Figure S11). Overall, these results indicate that *in vivo* ASO-123 delivery facilitated OHC survival in the low- and mid-frequency regions of the cochlea.

To determine whether ASO-123 can rescue KCNQ4 currents in OHCs, we used the voltage-clamp technique to compare KCNQ4 currents in OHCs across WT, untreated, and 15-μg ASO-123-treated *Kcnq4*$^{W277S/+}$ mice at P28 (Figure 5C). Consistent with previous reports,[7,54,55] OHCs from WT mice exhibited a characteristic $I_{K,n}$ current in response to a hyperpolarizing step pulse of −120 mV (Figure 5D). The OHCs of *Kcnq4*$^{W277S/+}$ mice, however, lacked this current, confirming that KCNQ4 mediates $I_{K,n}$. Notably, when we examined the OHCs of ASO-123-treated *Kcnq4*$^{W277S/+}$ mice, we observed a partial recovery of the $I_{K,n}$ current (Figure 5D). We then analyzed the properties of $K^+$ channels in OHCs in greater detail. While WT OHCs showed $I_{K,n}$ currents with an amplitude of −840 ± 142 pA ($n = 4$), *Kcnq4*$^{W277S/+}$ OHCs showed a significantly reduced amplitude of 5.11 ± 9.92 pA ($n = 4$) (Figures 5E and 5F). ASO-123 treatment partially restored this $I_{K,n}$ current to −96.7 ± 49.1 pA ($n = 4$) (Figures 5E and 5F). Furthermore, when we performed tail current amplitude measurements to assess voltage-activated $K^+$ channel gating and conductance, we observed a pronounced rightward-shift in the activation curve of *Kcnq4*$^{W277S/+}$ OHCs compared with WT (Figure 5G). WT OHCs exhibited a half-maximal activation voltage ($V_{1/2}$) of −81.3 ± 0.72 mV ($n = 4$), while *Kcnq4*$^{W277S/+}$ OHCs had a $V_{1/2}$ of −18.9 ± 1.68 mV ($n = 4$) (Figure 5H). *Kcnq4*$^{W277S/+}$ OHCs treated with ASO-123, however, showed a leftward-shift in their activation curve compared with untreated *Kcnq4*$^{W277S/+}$ OHCs and a significantly improved $V_{1/2}$ of −38.4 ± 1.65 mV ($n = 4$) (Figures 5G and 5H). Finally, we measured resting membrane potential (RMP) because it is a critical parameter associated with OHC stress under physiological conditions and because prolonged membrane depolarization can lead to OHC degeneration in both mice and humans carrying pathogenic *KCNQ4* mutations.[4,6,7,55] Consistent with previous reports, WT OHCs exhibited an RMP of −67.7 ± 2.17 mV ($n = 4$) (Figure 5I). In contrast, *Kcnq4*$^{W277S/+}$ OHCs showed a significantly depolarized RMP of −40.4 ± 4.50 mV ($n = 4$). Remarkably, ASO-123-treated *Kcnq4*$^{W277S/+}$ OHCs showed an RMP of −59.9 ± 3.03 mV ($n = 4$), which represented a significant recovery toward that of WT OHCs (Figure 5I). These RMP changes were directly linked to a rescue of OHC electromotility, which we confirmed by OHC circuit modeling (Figure S12). Compared with *Kcnq4*$^{W277S/+}$ OHCs, ASO-123-treated *Kcnq4*$^{W277S/+}$ OHCs exhibited a 2-fold increase in electromotility across all tested frequencies (Figure S12H). Together, these electrophysiological findings indicate that ASO-123 treatment partially restored KCNQ4 function and RMP in OHCs, validating its therapeutic efficacy.

### Transcriptomic changes reflect the efficacy of ASO treatment in *Kcnq4*$^{W277S/+}$ mice

To comprehensively evaluate the transcriptomic changes in *Kcnq4*$^{W277S/+}$ mice induced by ASO administration, we conducted RNA sequencing of cochleae from non-injected *Kcnq4*$^{+/+}$, *Kcnq4*$^{W277S/+}$, NT-ASO (15 μg)-treated, and ASO-123 (15 μg)-treated *Kcnq4*$^{W277S/+}$ mice at P28. ASO injections were performed between P1 and P3 via the RWM. After performing a principal-component analysis on the resulting RNA sequencing data, we found that *Kcnq4*$^{W277S/+}$ mice injected with ASO-123 clustered closer to *Kcnq4*$^{+/+}$ mice than to untreated or NT-ASO-injected *Kcnq4*$^{W277S/+}$ mice (Figure 6A). In a differentially expressed gene (DEG) analysis (significance determined as Benjamini-Hochberg adjusted $p < 0.05$), we found substantial transcriptomic changes in ASO-123-treated *Kcnq4*$^{W277S/+}$ mice compared with untreated and NT-ASO-treated controls. We observed minimal DEGs in the comparison between ASO-123-treated *Kcnq4*$^{W277S/+}$ and *Kcnq4*$^{+/+}$ mice (Figure 6B). These findings suggest that ASO-123 effectively restores the transcriptomic profile of *Kcnq4*$^{W277S/+}$ mice. To identify relevant biological processes implicated by DEGs, we performed a hierarchical clustering of significant DEGs and identified four specific clusters (Figure 6C). Table S5 contains the full list of DEGs for each cluster. The five genes in Cluster1 (*Dio2*, *Atg4a-ps*, *Ccrl2*, *Col20a1*, and *Fst*)

(gene count within a term divided by total genes). Colors represent adjusted *p* values, and sizes correspond to the number of DEGs associated with each GO term. (E) Heatmap representing the gene set variation analysis (GSVA) results. Columns represent samples, and rows indicate tested gene sets. Colors indicate normalized enrichment scores (NES). (F) Bar plots displaying the transcripts per million (TPM) values of representative target genes from the Toll-like receptor 3, 7, and 9 signaling pathways across the four groups. Data are shown as mean ± SD. Statistical significance was determined via two-way ANOVA with Bonferroni's corrections for multiple comparisons. ns, not significant. (G) Bar plots showing TPM values for candidate off-target genes across the four groups. Data are presented as mean ± SD. Statistical significance was determined via two-way ANOVA with Bonferroni's corrections for multiple comparisons. ns, not significant.

were not enough to allow us to detect any significantly enriched biological processes. Cluster 2 DEGs were upregulated in untreated and NT-ASO-treated *Kcnq4*$^{W277S/+}$ mice but downregulated following ASO-123 treatment, approaching levels observed in WT mice. These genes were associated with cell cycle and nuclear division, suggesting a compensatory response to cellular degeneration. Cluster 3 DEGs, which were downregulated in untreated and NT-ASO-treated *Kcnq4*$^{W277S/+}$ mice, encompass genes restored following ASO-123 treatment. These genes are involved in cilium assembly, microtubule bundle formation, and membrane potential regulation. Proper cilium assembly and microtubule bundle formation are associated with hair cell polarity and OHC electromotility,[56,57] while KCNQ4 function is essential for OHC membrane potential regulation. Cluster 4 DEGs, which were expressed at similar levels between untreated and ASO-123-treated *Kcnq4*$^{W277S/+}$ mice, are involved in innate immune responses and anti-viral responses. This suggests that ASO-123 did not evoke a significant innate immune response (Figure 6D). We also performed a gene set variation analysis (GSVA) to confirm the functional restoration at the individual sample level (Figure 6E). This revealed that genes involved in potassium ion transport and hearing maintenance were coordinately downregulated in untreated and NT-ASO-treated *Kcnq4*$^{W277S/+}$ mice and restored in response to ASO-123 treatment. Collectively, these findings confirm that ASO-123 restores various biological processes required for hearing maintenance without triggering a significant innate immune response.

Since ASOs can elicit *in vivo* toxicity by activating the innate immune system, particularly via the Toll-like receptor (TLR) 3, 7, and 9 signaling pathways,[58–60] we examined the expression of representative target genes from these pathways. We did not, however, observe any significant differences in TLR target gene expression across untreated, NT-ASO-treated, and ASO-123-treated *Kcnq4*$^{W277S/+}$ mice (Figure 6F). We also examined the expression levels of several candidate off-target genes identified via *in silico* prediction, including *Habp4* (Table S2) and four genes from the *Kcnq* family. The expression of these genes remained similar across untreated, NT-ASO-treated, and ASO-123-treated *Kcnq4*$^{W277S/+}$ mice (Figure 6G). Furthermore, we conducted a detailed analysis of 284 significantly downregulated DEGs (Benjamini-Hochberg adjusted $p < 0.05$) in ASO-123-treated *Kcnq4*$^{W277S/+}$ mice compared with NT-ASO-treated mice. These DEGs were categorized into two groups (Figure S13A). The first group included genes that were significantly upregulated in NT-ASO-injected *Kcnq4*$^{W277S/+}$ mice relative to WT mice, but whose expression was reversed by ASO-123 treatment in *Kcnq4*$^{W277S/+}$ mice. We designated these as “rescued genes” (141 genes). The second group contained genes that were not differentially expressed between NT-ASO-treated *Kcnq4*$^{W277S/+}$ and WT mice. We designated these as “potential off-target genes” (143 genes). When we compared their $\log_2$(fold change) ($\log_2$FC) values, we found more pronounced downregulation in the Rescued gene group than in the potential off-target gene group (average $\log_2$FC: $-0.410406$ vs. $-0.292258$, respectively). Notably, in the Rescued gene group, one gene exhibited a greater than 75% reduction in expression ($\log_2\text{FC} < -2$), and 10 genes exhibited greater than 50% reductions in expression ($\log_2\text{FC} < -1$). In contrast, no gene in the potential off-target group showed a greater than 50% reduction, and only three genes showed a greater than 30% reduction ($\log_2\text{FC} < -0.5$). This suggests ASO-123 administration triggered minimal off-target effects (Figure S13B). Overall, these findings indicate that ASO-123 treatment in the inner ear did not activate TLR 3, 7, or 9 signaling pathways and induced minimal off-target effects.

## DISCUSSION

Here, we employed an allele-specific ASO approach to mitigate progressive hearing loss in *Kcnq4*$^{W277S/+}$ mice, which are a model for human DFNA2. Through *in vitro* screening, we identified ASO-123, which preferentially knocks down the *Kcnq4* W277S allele over the WT allele with demonstrated safety and a minimal off-target profile. Local delivery of this ASO to *Kcnq4*$^{W277S/+}$ mice at P1–P3 via RWM injection significantly ameliorated progressive hearing loss, particularly in the low and mid-frequency regions, with improvements persisting up to 7 weeks post-injection. These therapeutic effects were accompanied by enhanced OHC survival and function. Our study provides clear proof-of-concept for the therapeutic potential of RNase-H1-dependent, allele-preferential ASOs for treating hereditary hearing loss.

Importantly, we observed that this gapmer ASO approach targeting the dominant-negative *Kcnq4* mutation yielded functional outcomes comparable with our previous allele-specific CRISPR-Cas9-based approach.[13] Although SpCas9-mediated allele disruption generally results in permanent effects, the degree of hearing loss alleviation over a 7-week period and the durability of the therapeutic benefits were similar between the two strategies. Furthermore, since ASOs primarily target mRNA and exert their effects over relatively short periods, they can circumvent most of the safety concerns associated with unintended, permanent DNA modifications at both on-target and off-target sites that are inherent to CRISPR-Cas9 systems. Collectively, our findings indicate that ASOs are a promising and potentially safer alternative therapeutic strategy for autosomal dominant hearing loss primarily affecting OHCs.

While our allele-preferential ASO significantly improved hearing loss in the low- and mid-frequency regions, we observed limited improvement in high-frequency regions. This regional variation likely reflects the spatiotemporal regulation of *Kcnq4* expression. In mice, *Kcnq4* expression begins in the basal cochlear turn at embryonic day 18.5, gradually progressing toward the apical turn.[48] Consequently, ASO delivery during the P1–P3 window may be too late to effectively rescue OHC function and survival in the basal turn. Since OHC degeneration in *Kcnq4*$^{W277S/+}$ mice progresses from base to apex, it is also possible that the current ASO treatment was insufficient to overcome the dominant-negative effects of mutant *Kcnq4* in the basal turn. Future studies will be necessary to optimize ASO design using stereopure phosphorothioate bonds to enhance allelic discrimination[61] and by incorporating phosphodiester bonds in place of phosphorothioate bonds in specific wing positions to maximize gapmer ASO tolerability.[62] Such changes could improve outcomes related to high-frequency hearing, while concurrently expanding the therapeutic index. Moreover, given that hearing loss in human DFNA2 patients typically begins in their 10s–30s as mild-to-moderate hearing loss and does not progress to a severe level until their 40s–60s,[4,63,64] we expect that the therapeutic time window for human DFNA2 patients would be broader than that observed in our DFNA2 mouse model, which exhibits relatively rapid progression of hearing loss. This supports the potential for successful clinical translation of ASO therapy.

Our deep sequencing and RT-PCR analyses revealed that, while ASO-123 preferentially suppressed mutant transcripts, there was also some reduction in *Kcnq4* WT transcripts, particularly at the higher dose. Fortunately, the *Kcnq4* gene shows a low probability of loss-of-function intolerance (pLI) score (0.02; gnomAD v.4.1.0).[65] This, coupled with the absence of hearing loss in heterozygous *Kcnq4* knockout mice,[7] suggests that *Kcnq4* is unlikely haploinsufficient and a partial reduction of WT transcripts might be well-tolerated. Nonetheless, careful consideration of the dosage sensitivity or haploinsufficiency of the target gene, along with precise dose optimization, remains crucial for successful and safe treatment.[66]

The therapeutic effects of ASO-123 persisted for up to 7 weeks post-injection but declined progressively, reflecting the gradual consumption and degradation of RNase-H1-dependent ASOs bound to target transcripts (Figures 3F–3H). This temporal limitation will necessitate regular dosing, as with other current clinical ASO drugs, which require maintenance therapy every 2–3 months.[30,31,36] In this study, we used RWM injection for local ASO delivery to the inner ear because this method gave greater therapeutic efficiency compared with other methods, such as intratympanic injection or topical-tympanic membrane application.[37] However, RWM injection is not ideal in a clinical setting for humans, because it would require repeated invasive surgical procedures either via a transcanal or transmastoid approach. For future clinical translation, the development of a reliable and less-invasive method for ASO delivery to the inner ear—such as strategies to transport systemically administered ASOs across the blood-labyrinth barrier—will be essential.

Our findings have broad implications for treating *KCNQ4*-associated DFNA2. Most deafness-associated mutations in *KCNQ4* are missense variants caused by single nucleotide changes, the majority of which presumably operate via dominant-negative mechanisms rather than haploinsufficiency.[4,10] For the *KCNQ4* p.W276S mutation specifically, population frequency data (0.000001695; gnomAD v.4.1.0) suggest that a considerable number of individuals may be at risk of developing hearing loss due to this mutation and could potentially benefit from the strategy demonstrated in this study. Moreover, in combination with long-read sequencing, allele-specific ASOs could be used to target various SNPs in *cis* configurations with individual pathogenic dominant-negative or gain-of function mutations, offering multiple target options even for mutations in regions unfavorable for direct allele-specific targeting.[36] Our study provides a compelling proof-of-concept for developing ASO therapies for genetic hearing loss, while also establishing important groundwork for future clinical translation.

## MATERIALS AND METHODS

### ASOs

The ASOs used in this study were synthesized and purified by Qmine (Suwon, Korea). These 16–18 base (16-18-mer) oligonucleotides have a gapmer structure, consisting of 7–8 bases of 2′-deoxyribonucleotides in the middle (gap) and 3–6 nucleotides at the 5′ and 3′ ends (wings) that are modified at the 2′-O position of ribose with a MOE group. All nucleotides were linked by a phosphorothioate backbone, and all cytosine bases were methylated at the 5′ position. Oligonucleotides for both *in vitro* and *in vivo* experiments were reconstituted with sterile, filtered PBS (Thermo Fisher Scientific, catalog no. 10010023) in a sterile hood and stored at −20°C until use. The sequences and chemistry of the oligonucleotides used in this study are presented in Table S1. NT-ASO sequences that do not target any genes in either the mouse or human genomes were obtained from previously published studies (NT-ASO1[67]; NT-ASO2[31,68]).

### Plasmid construction

WT cDNAs of mouse *Kcnq4* (catalog no. MR223106) and human KCNQ4 (catalog no. RC220242) were purchased from OriGene Technologies and subcloned into the pENTR-D-TOPO vector (Invitrogen, catalog no. K240020). LR clonase (Invitrogen, catalog no. 11791019) was used for mammalian expression vector construction, according to the manufacturer's instructions. A FLAG tag was added to the N terminus of mouse *Kcnq4* (pQCXIP-FLAG-mouse *Kcnq4*), and a Myctag was added to the N terminus of human *KCNQ4* (pRK5-Myc-human *KCNQ4*). The mouse *Kcnq4* p.W277S and human *KCNQ4* p.W276S mutant clones were generated via PCR-based site-directed mutagenesis using the Quick Change-II XL site-directed mutagenesis kit (Agilent Technologies, catalog no. 200521).

### Cell culture and transfection

HEK293T or HeLa cells were cultured in Dulbecco's modified essential medium (Gibco BRL, catalog no. 11965092) supplemented with 10% fetal bovine serum (Sigma, catalog no. F2442) and penicillin (50 IU/mL)-streptomycin (50 μg/mL) (Gibco BRL, catalog no. GIB-15410-122) at 37°C in a 5% $CO_2$ incubator.

Transfection of plasmids and ASOs was performed using Lipofectamine 2000 (Invitrogen, catalog no. 11668019) according to the manufacturer's instructions. Briefly, HEK293T cells were seeded in 6-well poly-D-lysine-coated plates at a density of 650,000–750,000 cells per well. From 18 to 24 h post-seeding, a 250-μL mixture containing 1 μg (human *KCNQ4*) or 2 μg (mouse *Kcnq4*) of target plasmid and candidate ASOs at the indicated final concentrations in culture medium and Opti-MEM reduced serum medium (Gibco BRL, catalog no. 31985070) was prepared. Separately, 5 μL (human *KCNQ4*) or 10 μL (mouse *Kcnq4*) of Lipofectamine 2000 was diluted in Opti-MEM to a total volume of 250 μL. Both mixtures were incubated for 5 min. Then, the two mixtures were combined, incubated for an additional 20 min, and added to the cells. Cells were harvested

48 h post-transfection for protein-level analysis or 24 h post-transfection for RNA-level analysis.

### Immunoblotting

Immunoblotting was performed as previously described.[69] Briefly, 48 h after transfection, protein samples were harvested, suspended in a sodium dodecyl sulfate (SDS) buffer, and then separated by SDS-polyacrylamide gel electrophoresis. The separated proteins were transferred to a nitrocellulose membrane and blotted with appropriate primary and secondary antibodies after blocking with 5% skim milk:anti-FLAG primary antibody (1:1,000, Cell Signaling Technology, catalog no. 8146), anti-Myc primary antibody (1:1,000, Cell Signaling Technology, catalog no. 2276), HRP anti-β-actin primary antibody (1:2,000, Abcam, catalog no. ab49900), and HRP anti-isotype secondary antibody (1:2,000, Cell Signaling Technology, catalog no. 7076P2). Protein band signals were captured using the Super Signal West-Pico Kit (Thermo Scientific, catalog no. 34579) and quantified using ImageJ.

### *In vitro* ASO toxicity assay

We employed the Caspase-Glo 3/7 assay (Promega, catalog no. G8090) for high-throughput analysis of ASO-mediated caspase activation. Briefly, HeLa cells were seeded in 96-well plates at a density of 16,000–18,000 cells per well, 18–24 h prior to transfection. Cells were then transfected with various concentrations of ASOs using 0.5 μL of Lipofectamine 2000 per well and incubated for an additional 8 h. After the incubation, equal volumes of Caspase-Glo 3/7 reagent were added directly to the wells, incubated for 30 min, and the resulting luminescence was measured using a Centro XS$^3$ LB 960 Microplate Luminometer (Berthold). The background signal was measured in wells containing only medium without cells. The average background signal was then subtracted from the signal in the ASO- or mock-treated wells. Relative caspase activity was calculated as (ASO-treated sample signal – average background signal)/(average mock-treated sample signal – average background signal).

### Off-target profiling

The ASO-123, nusinersen, and inotersen subsequences were computationally generated using a custom Python script by progressively trimming the ends from the full-length sequences until they reached 15–16 nt in length. BWA (v.0.7.17)[70] was used to align the full-length sequences and subsequences to the reference genome of each corresponding species (GRCm39 for ASO-123 and GRCh38 for nusinersen and inotersen).

### Mice

All animal experiments were reviewed and approved by the Institutional Animal Care and Use Committee of Yonsei University College of Medicine (no. 2020-0333). Mice were housed under pathogen-free conditions with a 12-h light cycle lasting from 8:00 a.m. to 8:00 p.m. with *ad libitum* access to water and irradiated rodent chow (LabDiet, catalog no. 0006972). The generation of the *Kcnq4* p.W277S knockin mouse model (C57BL/6N) was previously described.[13] For mouse genotyping, genomic DNA was extracted from toe cut samples and subjected to RFLP analysis. Briefly, PCR was performed using the appropriate primers (*Kcnq4*-genotype-fwd: 5′-GCATTCCTAGGG GTCTTTCC-3′; *Kcnq4*-genotype-rev: 5′-CATCAGGTTCTTGC-GAACCT-3′). Then, the PCR products were digested with NdeI (NEB, catalog no. R0111S) for 1–2 h at 37°C and subjected to 1.5% agarose gel electrophoresis to determine genotype.

### Inner ear injection

ASOs were injected into the inner ear of *Kcnq4* p.W277S heterozygous pups at P1–P3. After the pups were anesthetized by hypothermia, a post-auricular incision was made to expose the tympanic bulla. One microliter of ASO was injected into the cochlea through the round window using a glass pipette and a Nanoliter2020 Injector (World Precision Instruments, Hertfordshire, UK) at a steady rate of 250 nL/min. Following the injection, the incision was sutured with Nylon 6-0, and the pup was placed on a heating pad for at least 10 min until full recovery of consciousness.

### RNA extraction and RT-PCR

RT-PCR was performed as described previously.[71] For RNA extraction, mouse cochleae were dissected from temporal bone and the vestibule and semicircular canals were removed. Total RNA was extracted from cochleae or harvested cells using TRIzol (Invitrogen, catalog no. 15596026), and DNA contamination was eliminated via incubation of the total RNA with DNase I (Invitrogen, catalog no. 18068015). Then, 1 μg of total RNA was reverse-transcribed using the RNA-to-cDNA EcoDry Premix (Double Primed) kit (Takara, catalog no. 639548) according to the manufacturer's instructions. One microliter of the RT product was used for SYBR RT-PCR with the TB Green Premix Ex Taq II (Tli RNaseH Plus) qPCR Mix (Takara, catalog no. RR820A) and appropriate primers (*Kcnq4*-RT-PCR-fwd: 5′-GGAAACCCTTCTGTGTCATCGA-3′; *Kcnq4*-RT-PCR-rev: 5′-TGTGCCCGCAGCTATCACT-3′; *Actb*-RT-PCR-fwd: 5′-GAGACCTTCAACACCCCAGC-3′; *Actb*-RT-PCR-rev: 5′-AT GTCACGCACGATTTCCC-3′; *KCNQ4*-RT-PCR-fwd: 5′-TGCGACC GTACGACGTGAAG-3′; *KCNQ4*-RT-PCR-rev: 5′-CAATTTGGTCC ACCCGAGTTTGC-3′; *GAPDH*-RT-PCR-fwd: 5′-AAGGTGAAGGT CGGAGTCAACGG-3′; *GAPDH*-RT-PCR-rev: 5′-CCACTTGATTTT GGAGGGATCTC-3′). The $2^{-\Delta\Delta CT}$ method was used for relative quantification during RT-PCR data analysis with *Actb* (mouse cochleae) or *GAPDH* (HEK293T cells) as the housekeeping genes.

### RFLP analysis

Total RNA was extracted from cochleae, and cDNA synthesis was conducted as described above. The *Kcnq4* target region, encompassing both the c.810C>A (synonymous) and c.830G>C (missense) mutations, was amplified via PCR using *Kcnq4*-RFLP-fwd (5′-AA CATCTTTGCTACGTCCGC-3′) and *Kcnq4*-RFLP-rev (5′-GCAGGG CAAAGAAGGAGATG-3′). Then, the resulting PCR products were incubated with NdeI (NEB, catalog no. R0111S) for 1.5 h at 37°C. The digested products were then separated and visualized via 1.5% agarose gel electrophoresis. Band intensities were quantified using ImageJ, with the intensity of the *Actb* band serving as a loading control.

### Targeted deep sequencing

Total RNA was extracted from cochleae and used to produce cDNAs according to the methods described above. Amplification of target site sequences was carried out using a two-step nested PCR protocol with *Kcnq4*-deep-seq-fwd (5′- ACACTCTTTCCCTACA CGACGCTCTTCCGATCTTATGCGCACAGTAAGGAGCT-3′) and *Kcnq4*-deep-seq-rev (5′-GTGACTGGAGTTCAGACGTGTGCT CTTCCGATCTGCAGGGCAAAGAAGGAGATG-3′) primers for the first round (PCR1). Then, in the second round (PCR2), Illumina adapters and unique barcoding indices were added to the PCR1 products from each sample. Subsequently, pooled PCR2 products were visualized on 1.5% agarose gels and purified using a TIANGEN purification kit (catalog no. 4,992,197). A total of 150 bp paired-end reads was generated using the Illumina NovaSeq 6000 platform. Data analysis of the original sequencing fastq files was conducted with Cutadapt (v.5.1)[72] and DADA2 (v.1.26).[73] First, adaptor and primer sequences were trimmed using Cutadapt. Then, low-quality reads were filtered out, and forward and reverse reads were merged. Chimeric reads were removed to generate the final amplicon sequence variant (ASV) table using DADA2. For the calculation of read counts, WT reads (c.830G) not carrying the upstream synonymous mutation (c.810C) (5′-CCTATGCCGACTCGCTCTGGTGGGGG-3′) and mutant reads (c.830G>C) harboring the upstream synonymous mutation (c.810C>A) (5′-CATATGCCGACTCGCTCTGGTCGG GG-3′) were counted in the final ASV table.

### RNA sequencing

After dissecting cochleae from the temporal bone and removing the vestibule and semicircular canals, the remaining tissues were homogenized. Total RNA was extracted using TRIzol (Invitrogen, catalog no. 15596026) and then cleaned with the RNeasy mini kit (QIAGEN, catalog no. 74,106) according to the manufacturer's instructions. The concentration of the resulting total RNA was measured using Quant-IT RiboGreen (Invitrogen, catalog no. R11490). Total RNA integrity (RIN) was assessed with the TapeStation RNA ScreenTape device (Agilent Technologies, catalog no. 5067-5576). Only high-quality RNA preparations ($\text{RIN} \geq 7.0$) were used for RNA library construction. RNA sequencing was performed by Macrogen (Seoul, Korea). Libraries were independently prepared from 1 μg of total RNA per sample using the Illumina TruSeq stranded mRNA sample prep kit (Illumina, catalog no. RS-122-2101). Then, poly(A)-containing mRNA molecules were purified using poly(T)-attached magnetic beads. Following purification, the mRNAs were fragmented using divalent cations and elevated temperature. The cleaved RNA fragments were then copied into first-strand cDNAs using SuperScript II reverse transcriptase (Invitrogen, catalog no. 18064014) and random primers. This was followed by second-strand cDNA synthesis using DNA polymerase I, RNase H, and deoxynucleotide triphosphates. The resulting cDNA fragments were then subjected to an end-repair process, the addition of a single "A" base, and the ligation of adapter molecules. The products were then purified and PCR-enriched to create each final cDNA library. The libraries were quantified using KAPA library quantification kits for Illumina sequencing platforms according to the qPCR quantification protocol and qualified using the TapeStation D1000 ScreenTape device (Agilent Technologies, catalog no. 5067-5582). Indexed libraries were then read on the Illumina NovaSeq 6000 (Illumina) platform via 2 × 101-bp paired-end sequencing.

RNA sequencing analysis was performed according to a previously published workflow.[74] Raw sequencing quality was assessed using FastQC (v.0.12.1). Adapter trimming and quality filtering were performed via Trimmomatic (v.0.40).[75] Reads were aligned to GRCm39 with HISAT2 (v.2.2.1),[76] retaining only those that were uniquely mapped. Total exon reads were counted by FeatureCounts (v.2.0.6).[77] Downstream analyses were performed in R (v.4.2.1). Differential gene expression and Gene Ontology analysis were conducted with DESeq2 (v.1.38.3)[78] and ClusterProfiler (v.4.6.2),[79] respectively. The GSVA package (v.1.46.0)[80] was used for GSVA. Gene lists related to potassium ion transport (GO:0006813) were obtained from the MSigDB database (MSigDB: https://www.gsea-msigdb.org/gsea/msigdb), while gene lists associated with hearing maintenance were acquired from a previous publication (Table S6).[81]

### Hybridization ELISA

Cochleae and ipsilateral brain hemispheres from ASO-123-injected mice were snap-frozen in liquid nitrogen and stored at −80°C until analysis. The tissues were subjected to hybridization ELISA as previously described, with minor modifications.[82,83] The capture probe was a 26-mer DNA oligonucleotide (5′-GATAACCGTCTCGCTC TGGTCGGGGA-3′) biotinylated at the 3′ end, and the detection probe was a 9-mer DNA oligonucleotide (5′-ACGGTTATC-3′) labeled with digoxigenin at the 5′ end. Both oligonucleotides were synthesized by Integrated DNA Technologies (Coralville, IA). Polystyrene plates were coated with NeutrAvidin (ThermoFisher Scientific, catalog no. 31000) in PBS and incubated overnight at room temperature. The plates were then blocked with SuperBlock T20 (Thermo Fisher Scientific, catalog no. 37536). Capture probes and experimental samples were mixed and hybridized in solution at 37°C for 1 h. A 150-μL aliquot of the hybridization mixture was transferred to the NeutrAvidin-coated wells and incubated for an additional 30 min at 37°C, followed by four washes with TBST. For detection, 75 units of T4 DNA ligase (5 U/μL, Thermo Fisher Scientific, catalog no. EL0011) was combined with 50 nM detection probe in 100 μL of ligation buffer and added to each well. Then, the plates were incubated at room temperature for 2 h. After two washes with TBST and three washes with distilled water, anti-digoxigenin alkaline phosphatase (AP)-conjugated antibody (Merck, catalog no. 11093274910) was added and incubated for 30 min. After four additional washes with TBST, AttoPhos AP fluorescent substrate (Promega, catalog no. S1001) was added. The resulting fluorescence intensities were measured using a CLARIOstar plate reader (BMG Labtech, Ortenberg, Germany) at excitation and emission wavelengths of 435/10 and 560/10 nm, respectively.

### *ABRs and DPOAEs*

ABR thresholds were assessed in a sound-proof chamber using Tucker-Davis Technologies (TDT) RZ6 digital signal processing hardware and BioSigRZ software (Alachua, FL). Electrodes were positioned at the vertex and ventrolateral to both ears of anesthetized mice. Click and tone burst stimuli were generated at different frequencies (6, 12, 18, 24, and 30 kHz) using SigGenRZ software and an RZ6 digital signal processor. These stimuli were delivered to the ear canal using a multi-field 1 (MF1) magnetic speaker (TDT). The stimulus intensity was varied from 20 to 90 dB SPL in 5 dB increments. The ABR signals were fed into a low-impedance Medusa Biological Amplifier System (RA4LI, TDT) and then to the RZ6 digital signal processing hardware. The recorded signals were filtered with a 0.5- to 1-kHz band-pass filter, and the ABR waveforms in response to 512 tone bursts were averaged. BioSigRZ software was used to determine ABR thresholds for each frequency, and peak amplitudes (mV) were calculated using click-evoked ABR waveforms as input/output (I/O) functions with an increasing stimulus level (20–90 dB SPL).

For DPOAE measurements, a combination of TDT microphone-speaker systems was used. Primary stimulus tones were generated using an RZ6 digital signal processor with SigGenRZ software and delivered through a custom probe with an ER 10B+ microphone (Etymotic, IL) and MF1 speakers placed in the ear canal. The primary tones had a frequency ratio (f2/f1) of 1.2. Target frequencies included 6, 12, 18, 24, and 30 kHz. The intensity of f2 was the same as f1 (L1 = L2). The resulting sounds from the primary tones were recorded using an RZ6 digital signal processor. DPOAE I/O functions were determined at specific frequencies with an f2/f1 ratio of 1.2 and L1 = L2. The intensity of the primary tones was increased from 20 to 80 dB SPL in 5-dB SPL increments. Fast Fourier transform was performed for each primary tone using DP-grams. For the I/O function intensity, BioSigRZ software was used to determine the average spectra of the two primaries, the 2f1-f2 distortion products, and the noise floor.

### *Immunofluorescence and confocal microscopy*

Mouse inner ear tissues were dissected from the temporal bone and fixed in 4% paraformaldehyde in PBS overnight at 4°C. Fixed cochleae were decalcified with 200 mM EDTA (iNtRON, catalog no. IBS-BE002) for 2–3 days at 4°C. Then, the samples were dissected under a microscope to separate the three turns (apex, mid, and base) of the organ of Corti. Simultaneously, the samples were permeabilized and blocked with 5% donkey serum (Sigma, catalog no. D9663), 0.1% BSA (Sigma, catalog no. A7030), and 0.1% Triton X-100 (Biosesang, catalog no. TR1020-500) in PBS for 1 h at room temperature. Then, the samples were incubated with anti-MYO7A (Proteus, catalog no. PTS-25-6790, 1:200), anti-fluorescein (Abcam, catalog no. ab19491, 1:200), anti-parvalbumin (Sigma, catalog no. P3088, 1:250), or anti-neurofilament H (Sigma, catalog no. AB5539, 1:1,000) primary antibodies overnight at 4°C. After three washes in PBS, the samples were incubated with an appropriate fluorophore-tagged secondary antibody (1:1,000), Alexa Fluor 594 phalloidin (Invitrogen, catalog no. A12381, 1:400), or DAPI (Bio-Rad, catalog no. 1,351,303, 1:100) for 2 h at room temperature. After secondary antibody incubation, the samples were again washed three times with PBS and mounted on slide glass with Dako Faramount Aqueous Mounting Medium (Dako, catalog no. S3023).

To make cross-sections, the fixed and decalcified cochleae or brains were embedded in paraffin, sectioned at 8 μm thickness, deparaffinized, rehydrated, and subjected to antigen retrieval through boiling in a Retrieve-all Antigen unmasking buffer (BioLegend, catalog no. 927,901, 1:100, Universal pH 8.0). The specimens were then permeabilized with 1% SDS in PBS for 10 min at room temperature and blocked in 5% donkey serum (Sigma, catalog no. D9663) and 0.1% BSA (Sigma, catalog no. A7030) in PBS for 1 h. Then, the samples were incubated at 4°C overnight in anti-fluorescein (Abcam, catalog no. ab19491, 1:200) and anti-Tuj1 (Tubb3) (BioLegend, catalog no. 801,201, 1:300) primary antibodies diluted in blocking buffer. After three washes in PBS, the samples were incubated for 2 h at room temperature in blocking buffer with the appropriate fluorophore-tagged secondary antibodies (1:1,000) and DAPI (Bio-Rad, catalog no. 1,351,303, 1:100). Then, they were mounted in Dako Faramount Aqueous Mounting Medium (Agilent Dako, catalog no. S3025).

Z-Stacked confocal images were obtained using a Carl Zeiss LSM780 microscope and processed as maximal-intensity projections using ZEN software. To quantify hair cell survival, MYO7A-positive cells per 100 μm length were counted in the apical (6–8 kHz region), mid (16–18 kHz region), and basal (32–34 kHz region) cochlear turns. To quantify SGN survival, Tuj1-positive cells per 10,000 $\mu m^2$ area were counted in Rosenthal's canal within the apical, mid, and basal cochlear turns. To quantify FAM fluorescence intensity in each cochlear region (apex, mid, and base), regions of interest (ROIs) were defined within the hair cells on reconstructed images. The mean fluorescence intensity of each ROI was measured using ImageJ. Background noise was estimated by measuring the mean fluorescence intensity in an area outside the hair cells and subtracted from the corresponding ROI values in each image.

### OHC electrophysiology

Organs of Corti from P28 mice were acutely isolated and prepared for electrophysiology as previously described.[84] First, the animals were anesthetized using Isofluran (Sigma, catalog no. 792632) and killed by decapitation. The bone surrounding the apical cochlear turn was removed, and the apical turn was carefully detached using forceps. It was then separated from the lateral cochlear wall, stria vascularis, modiolus, and tectorial membrane. The whole dissection procedure was performed in standard extracellular solution containing 144 mM NaCl, 5.8 mM KCl, 10 mM HEPES, 5.6 mM glucose, 0.7 mM $NaH_2PO_4$, 1.3 mM $CaCl_2$, 0.9 mM $MgCl_2$, and 10 mM sorbitol, and adjusted to pH 7.4 using NaOH. The cochlea was immobilized on a 12-mm diameter coverslip with a stainless-steel pin and Sylgard, before being mounted in an upright microscope ECLIPSE FN1 (Nikon, Japan).

Patch-clamp experiments were performed in standard whole-cell configurations as previously described.[85] All recordings were performed at room temperature (22°C–25°C). Microglass pipettes

(World Precision Instruments) were fabricated using a PP-830 single-stage glass microelectrode puller (Narishige, Japan) with a resistance of 2–5 MΩ. The liquid junction potential was rectified using an offset circuit prior to each recording. Currents were recorded using an Axopatch 700B amplifier and a Digidata 1550A interface, digitized at 20 kHz, and low-pass-filtered at 1 kHz using pClamp software 10.7 (Molecular Devices). The whole-cell voltage-clamp configuration was verified by measuring the series resistance to less than 10 MΩ, which was then compensated before each recording. To ensure a stable voltage clamp and maintain data integrity, only recordings with a steady-state leak current <50 pA at −80 mV and that met all of the following criteria were analyzed: seal resistance >4 GΩ, series resistance <10 MΩ with <15% drift, and membrane capacitance between 8 and 15 pF.

In the whole-cell voltage-clamp configuration, cells were held at −80 mV. Currents were evoked by 200-ms test pulses at −120 to 40 mV, and then a 100-ms post-pulse at −40 mV. The tail current amplitude was used to calculate the half-maximal activation voltage ($V_{1/2}$) by fitting it to the Boltzmann equation as follows:

$$\frac{G}{G_{\max}} = A_2 + \frac{A_1 - A_2}{1+e^{(V_h - V)/k}} \qquad \text{(Equation 1)}$$

wherein $G/G_{\max}$ is the normalized conductance calculated from the tail currents, V is the applied voltage, $V_h$ is the half-maximal activation voltage denoted as $V_{1/2}$ in the article, and k is the slope factor. $A_1$ and $A_2$ are the maximum and minimum values of the curve, respectively.

RMP was determined in current-clamp mode by averaging a 20-s gap-free recording.

The whole-cell patch-clamp experiment was conducted using a standard extracellular bath solution containing 144 mM NaCl, 5.8 mM KCl, 10 mM HEPES, 5.6 mM glucose, 0.7 mM $NaH_2PO_4$, 1.3 mM $CaCl_2$, 0.9 mM $MgCl_2$, and 10 mM sorbitol and adjusted to pH 7.4 using NaOH. The standard pipette solution contained 140 mM KCl, 10 mM HEPES, 2 mM EGTA, 3 mM Mg-ATP, and 1 mM $MgCl_2$, and was adjusted to pH 7.2 using KOH.

### OHC circuit modeling

The model of the OHC circuit was a slight modification of a previous model.[84] It assumes three main components underlie the major ionic conductance in OHCs: the mechanoelectrical transducer (MET) channel, the large-conductance $K^+$ channel $I_{K,n}$ identified as KCNQ4, and the capacitive current modulated by Prestin.

The closed OHC circuit can be expressed in the following equation:

$$C_m \frac{dV_m}{dt} + I_{MET} + I_K = 0. \qquad \text{(Equation 2)}$$

The non-linear OHC membrane capacitance can be expressed as follows:

$$C_m = C_{lin} + \frac{Q_{max}}{\alpha e^{\frac{V - V_{h,Pres}}{\alpha}} \left(1+e^{-\frac{V - V_{h,Pres}}{\alpha}}\right)^2}. \qquad \text{(Equation 3)}$$

The gating of the MET channel can be expressed as follows[86,87]:

$$n_{MET,\infty} = \frac{1}{1+e^{-\frac{\mu - x_0}{s_1}}\left(1+e^{-\frac{\mu - x_0}{s_0}}\right)} \qquad \text{(Equation 4)}$$

$$n_{MET} + \tau_{MET}\frac{dn_{MET}}{dt} = n_{MET,\infty} \qquad \text{(Equation 5)}$$

$$g_{MET}(\mu) = nG_{MET} \qquad \text{(Equation 6)}$$

$$I_{MET} = g_{MET}(\mu)(V_m - EP). \qquad \text{(Equation 7)}$$

The gating of the $K^+$ channel can be expressed as follows[54]:

$$n_{K,s/n,\infty} = \frac{1}{1+e^{-\frac{V_m - V_{h,K,s/n}}{s_{K,s/n}}}} \qquad \text{(Equation 8)}$$

$$n_K + \tau_K\frac{dn_K}{dt} = n_{K,\infty} \qquad \text{(Equation 9)}$$

$$g_K = n_K\, G_K \qquad \text{(Equation 10)}$$

$$\tau_{K,WT} = -0.1035 \times V_m + 9.563 \qquad \text{(Equation 11)}$$

$$\tau_{K,Het} = -0.1969 \times V_m + 10.35 \qquad \text{(Equation 12)}$$

$$\tau_{K,ASO} = -0.0780 \times V_m + 3.979 \qquad \text{(Equation 13)}$$

$$I_K = g_K(V_m - E_K). \qquad \text{(Equation 14)}$$

The power of electromotility was calculated using the following equation:

$$\Delta P = \frac{1}{2}\Delta C_m \Delta {V_m}^2. \qquad \text{(Equation 15)}$$

The differential equations were solved using a custom Python script that incorporated the NumPy and SciPy modules.[88,89] The parameters used in these equations appear in Table S7.

### Statistical analyses

Statistical differences between two groups were assessed with Student's t tests. Comparisons involving more than two groups were assessed via one- or two-way ANOVA using the GraphPad Prism 8.0 software (GraphPad Software, CA). The appropriate corrections for multiple comparisons are specified in the figure legends.

Two-sided *p* values of less than 0.05 were considered significant. All data in the figures are presented as mean ± SD.

## DATA AVAILABILITY

The main data supporting the results of this study are available within the paper and its supplemental information. The raw RNA and targeted deep sequencing data from this study were deposited in K-BDS (Korea BioData Station, https://kbds.re.kr) with accession IDs KAP241063 and KAP241541, respectively.

## ACKNOWLEDGMENTS

This work was supported by an MD-PhD/Medical Scientist Training Program grant through the Korea Health Industry Development Institute (KHIDI) (to S.H.J. and J. W.R.), a grant funded by the Ministry of Health & Welfare (RS-2024-00438709 and RS-2023-00261905 to H.Y.G., and RS-2024-00439403 to J.J), a National Research Council of Science & Technology (NST) grant by the Korea government (MSIT) (GTL24021-000 to J.B. and H.Y.G.), and the National Research Foundation of Korea (RS-2022-NR070578 and RS-2024-00509145 to J.B.). The graphical abstract was created in BioRender (https://www.biorender.com/).

## AUTHOR CONTRIBUTIONS

H.Y.G. and J.B. conceived and supervised the project. S.H.J., J.W.R., and H.Y.G. designed the experiments. S.H.J. conducted most of the *in vitro* and *in vivo* experiments. J.W.R. performed the electrophysiological experiments and OHC circuit modeling. S.H.J. conducted all bioinformatic analyses. K.S.O. provided plasmids for the *in vitro* experiments. Y.J.K. supplied ASOs for both *in vitro* and *in vivo* experiments. S.H.J. and J.W.R. wrote the initial manuscript. All authors reviewed and edited the manuscript.

## DECLARATION OF INTERESTS

Y.J.K is the founder and shareholder of Qmine Co., Ltd. Y.J.K has filed a patent related to the data presented in this manuscript.

## SUPPLEMENTAL INFORMATION

Supplemental information can be found online at https://doi.org/10.1016/j.ymthe.2025.08.044.

## REFERENCES

1. Chadha, S., Kamenov, K., and Cieza, A. (2021). The world report on hearing, 2021. Bull. World Health Organ. *99*, 242. https://doi.org/10.2471/blt.21.285643.
2. Morton, C.C., and Nance, W.E. (2006). Newborn hearing screening–a silent revolution. N. Engl. J. Med. *354*, 2151–2164. https://doi.org/10.1056/NEJMra050700.
3. Rim, J.H., Noh, B., Koh, Y.I., Joo, S.Y., Oh, K.S., Kim, K., Kim, J.A., Kim, D.H., Kim, H.Y., Yoo, J.E., et al. (2022). Differential genetic diagnoses of adult post-lingual hearing loss according to the audiogram pattern and novel candidate gene evaluation. Hum. Genet. *141*, 915–927. https://doi.org/10.1007/s00439-021-02367-z.
4. Oh, K.S., Roh, J.W., Joo, S.Y., Ryu, K., Kim, J.A., Kim, S.J., Jang, S.H., Koh, Y.I., Kim, D. H., Kim, H.Y., et al. (2023). Overlooked KCNQ4 variants augment the risk of hearing loss. Exp. Mol. Med. *55*, 844–859. https://doi.org/10.1038/s12276-023-00976-4.
5. Jang, S.H., Yoon, K., and Gee, H.Y. (2024). Common genetic etiologies of sensorineural hearing loss in Koreans. Genomics Inform. *22*, 27. https://doi.org/10.1186/s44342-024-00030-3.
6. Kubisch, C., Schroeder, B.C., Friedrich, T., Lütjohann, B., El-Amraoui, A., Marlin, S., Petit, C., and Jentsch, T.J. (1999). KCNQ4, a novel potassium channel expressed in sensory outer hair cells, is mutated in dominant deafness. Cell *96*, 437–446.
7. Kharkovets, T., Dedek, K., Maier, H., Schweizer, M., Khimich, D., Nouvian, R., Vardanyan, V., Leuwer, R., Moser, T., and Jentsch, T.J. (2006). Mice with altered KCNQ4 K+ channels implicate sensory outer hair cells in human progressive deafness. EMBO J. *25*, 642–652. https://doi.org/10.1038/sj.emboj.7600951.
8. Lee, S.Y., Choi, H.B., Park, M., Choi, I.S., An, J., Kim, A., Kim, E., Kim, N., Han, J.H., Kim, M.Y., et al. (2021). Novel KCNQ4 variants in different functional domains confer genotype- and mechanism-based therapeutics in patients with nonsyndromic hearing loss. Exp. Mol. Med. *53*, 1192–1204. https://doi.org/10.1038/s12276-021-00653-4.
9. Kamada, F., Kure, S., Kudo, T., Suzuki, Y., Oshima, T., Ichinohe, A., Kojima, K., Niihori, T., Kanno, J., Narumi, Y., et al. (2006). A novel KCNQ4 one-base deletion in a large pedigree with hearing loss: implication for the genotype-phenotype correlation. J. Hum. Genet. *51*, 455–460. https://doi.org/10.1007/s10038-006-0384-7.
10. Jung, J., Lin, H., Koh, Y.I., Ryu, K., Lee, J.S., Rim, J.H., Choi, H.J., Lee, H.J., Kim, H. Y., Yu, S., et al. (2019). Rare KCNQ4 variants found in public databases underlie impaired channel activity that may contribute to hearing impairment. Exp. Mol. Med. *51*, 1–12. https://doi.org/10.1038/s12276-019-0300-9.
11. Coucke, P.J., Van Hauwe, P., Kelley, P.M., Kunst, H., Schatteman, I., Van Velzen, D., Meyers, J., Ensink, R.J., Verstreken, M., Declau, F., et al. (1999). Mutations in the KCNQ4 gene are responsible for autosomal dominant deafness in four DFNA2 families. Hum. Mol. Genet. *8*, 1321–1328.
12. Van Camp, G., Coucke, P.J., Akita, J., Fransen, E., Abe, S., De Leenheer, E.M.R., Huygen, P.L.M., Cremers, C.W.R.J., and Usami, S.I. (2002). A mutational hot spot in the KCNQ4 gene responsible for autosomal dominant hearing impairment. Hum. Mutat. *20*, 15–19. https://doi.org/10.1002/humu.10096.
13. Noh, B., Rim, J.H., Gopalappa, R., Lin, H., Kim, K.M., Kang, M.J., Gee, H.Y., Choi, J. Y., Kim, H.H., and Jung, J. (2022). In vivo outer hair cell gene editing ameliorates progressive hearing loss in dominant-negative Kcnq4 murine model. Theranostics *12*, 2465–2482. https://doi.org/10.7150/thno.67781.
14. Lv, J., Wang, H., Cheng, X., Chen, Y., Wang, D., Zhang, L., Cao, Q., Tang, H., Hu, S., Gao, K., et al. (2024). AAV1-hOTOF gene therapy for autosomal recessive deafness 9: a single-arm trial. Lancet *403*, 2317–2325. https://doi.org/10.1016/s0140-6736(23)02874-x.
15. Wang, H., Chen, Y., Lv, J., Cheng, X., Cao, Q., Wang, D., Zhang, L., Zhu, B., Shen, M., Xu, C., et al. (2024). Bilateral gene therapy in children with autosomal recessive deafness 9: single-arm trial results. Nat. Med. *30*, 1898–1904. https://doi.org/10.1038/s41591-024-03023-5.
16. Mendia, C., Peineau, T., Zamani, M., Felgerolle, C., Yahiaoui, N., Christophersen, N., Papal, S., Maudoux, A., Maroofian, R., Patni, P., et al. (2024). Clarin-2 gene supplementation durably preserves hearing in a model of progressive hearing loss. Mol. Ther. *32*, 800–817. https://doi.org/10.1016/j.ymthe.2024.01.021.
17. Shubina-Oleinik, O., Nist-Lund, C., French, C., Rockowitz, S., Shearer, A.E., and Holt, J.R. (2021). Dual-vector gene therapy restores cochlear amplification and auditory sensitivity in a mouse model of DFNB16 hearing loss. Sci. Adv. *7*, eabi7629. https://doi.org/10.1126/sciadv.abi7629.
18. Ivanchenko, M.V., Hathaway, D.M., Klein, A.J., Pan, B., Strelkova, O., De-la-Torre, P., Wu, X., Peters, C.W., Mulhall, E.M., Booth, K.T., et al. (2023). Mini-PCDH15 gene therapy rescues hearing in a mouse model of Usher syndrome type 1F. Nat. Commun. *14*, 2400. https://doi.org/10.1038/s41467-023-38038-y.
19. Tao, Y., Lamas, V., Du, W., Zhu, W., Li, Y., Whittaker, M.N., Zuris, J.A., Thompson, D.B., Rameshbabu, A.P., Shu, Y., et al. (2023). Treatment of monogenic and digenic dominant genetic hearing loss by CRISPR-Cas9 ribonucleoprotein delivery in vivo. Nat. Commun. *14*, 4928. https://doi.org/10.1038/s41467-023-40476-7.
20. György, B., Nist-Lund, C., Pan, B., Asai, Y., Karavitaki, K.D., Kleinstiver, B.P., Garcia, S.P., Zaborowski, M.P., Solanes, P., Spataro, S., et al. (2019). Allele-specific gene editing prevents deafness in a model of dominant progressive hearing loss. Nat. Med. *25*, 1123–1130. https://doi.org/10.1038/s41591-019-0500-9.
21. Fu, Y., Foden, J.A., Khayter, C., Maeder, M.L., Reyon, D., Joung, J.K., and Sander, J. D. (2013). High-frequency off-target mutagenesis induced by CRISPR-Cas nucleases in human cells. Nat. Biotechnol. *31*, 822–826. https://doi.org/10.1038/nbt.2623.
22. Lin, Y., Cradick, T.J., Brown, M.T., Deshmukh, H., Ranjan, P., Sarode, N., Wile, B. M., Vertino, P.M., Stewart, F.J., and Bao, G. (2014). CRISPR/Cas9 systems have off-target activity with insertions or deletions between target DNA and guide RNA sequences. Nucleic Acids Res. *42*, 7473–7485. https://doi.org/10.1093/nar/gku402.
23. Shin, H.Y., Wang, C., Lee, H.K., Yoo, K.H., Zeng, X., Kuhns, T., Yang, C.M., Mohr, T., Liu, C., and Hennighausen, L. (2017). CRISPR/Cas9 targeting events cause complex deletions and insertions at 17 sites in the mouse genome. Nat. Commun. *8*, 15464. https://doi.org/10.1038/ncomms15464.
24. Kosicki, M., Tomberg, K., and Bradley, A. (2018). Repair of double-strand breaks induced by CRISPR-Cas9 leads to large deletions and complex rearrangements. Nat. Biotechnol. *36*, 765–771. https://doi.org/10.1038/nbt.4192.

25. Nelson, C.E., Wu, Y., Gemberling, M.P., Oliver, M.L., Waller, M.A., Bohning, J.D., Robinson-Hamm, J.N., Bulaklak, K., Castellanos Rivera, R.M., Collier, J.H., et al. (2019). Long-term evaluation of AAV-CRISPR genome editing for Duchenne muscular dystrophy. Nat. Med. *25*, 427–432. https://doi.org/10.1038/s41591-019-0344-3.

26. Haapaniemi, E., Botla, S., Persson, J., Schmierer, B., and Taipale, J. (2018). CRISPR-Cas9 genome editing induces a p53-mediated DNA damage response. Nat. Med. *24*, 927–930. https://doi.org/10.1038/s41591-018-0049-z.

27. Lek, A., Wong, B., Keeler, A., Blackwood, M., Ma, K., Huang, S., Sylvia, K., Batista, A. R., Artinian, R., Kokoski, D., et al. (2023). Death after High-Dose rAAV9 Gene Therapy in a Patient with Duchenne's Muscular Dystrophy. N. Engl. J. Med. *389*, 1203–1210. https://doi.org/10.1056/NEJMoa2307798.

28. Morales, L., Gambhir, Y., Bennett, J., and Stedman, H.H. (2020). Broader Implications of Progressive Liver Dysfunction and Lethal Sepsis in Two Boys following Systemic High-Dose AAV. Mol. Ther. *28*, 1753–1755. https://doi.org/10.1016/j.ymthe.2020.07.009.

29. Costa Verdera, H., Kuranda, K., and Mingozzi, F. (2020). AAV Vector Immunogenicity in Humans: A Long Journey to Successful Gene Transfer. Mol. Ther. *28*, 723–746. https://doi.org/10.1016/j.ymthe.2019.12.010.

30. Kim, J., Hu, C., Moufawad El Achkar, C., Black, L.E., Douville, J., Larson, A., Pendergast, M.K., Goldkind, S.F., Lee, E.A., Kuniholm, A., et al. (2019). Patient-Customized Oligonucleotide Therapy for a Rare Genetic Disease. N. Engl. J. Med. *381*, 1644–1652. https://doi.org/10.1056/NEJMoa1813279.

31. Kim, J., Woo, S., de Gusmao, C.M., Zhao, B., Chin, D.H., DiDonato, R.L., Nguyen, M.A., Nakayama, T., Hu, C.A., Soucy, A., et al. (2023). A framework for individualized splice-switching oligonucleotide therapy. Nature *619*, 828–836. https://doi.org/10.1038/s41586-023-06277-0.

32. Chen, X., Birey, F., Li, M.Y., Revah, O., Levy, R., Thete, M.V., Reis, N., Kaganovsky, K., Onesto, M., Sakai, N., et al. (2024). Antisense oligonucleotide therapeutic approach for Timothy syndrome. Nature *628*, 818–825. https://doi.org/10.1038/s41586-024-07310-6.

33. Dindot, S.V., Christian, S., Murphy, W.J., Berent, A., Panagoulias, J., Schlafer, A., Ballard, J., Radeva, K., Robinson, R., Myers, L., et al. (2023). An ASO therapy for Angelman syndrome that targets an evolutionarily conserved region at the start of the UBE3A-AS transcript. Sci. Transl. Med. *15*, eabf4077. https://doi.org/10.1126/scitranslmed.abf4077.

34. Shao, Y., Sztainberg, Y., Wang, Q., Bajikar, S.S., Trostle, A.J., Wan, Y.W., Jafar-Nejad, P., Rigo, F., Liu, Z., Tang, J., and Zoghbi, H.Y. (2021). Antisense oligonucleotide therapy in a humanized mouse model of MECP2 duplication syndrome. Sci. Transl. Med. *13*, eaaz7785. https://doi.org/10.1126/scitranslmed.aaz7785.

35. Viengkhou, B., Hong, C., Mazur, C., Damle, S., Gallo, N.B., Fang, T.C., Henry, K., Campbell, I.L., Kamme, F., and Hofer, M.J. (2024). Interferon-α receptor antisense oligonucleotides reduce neuroinflammation and neuropathology in a mouse model of cerebral interferonopathy. J. Clin. Invest. *134*, e169562. https://doi.org/10.1172/jci169562.

36. Ziegler, A., Carroll, J., Bain, J.M., Sands, T.T., Fee, R.J., Uher, D., Kanner, C.H., Montes, J., Glass, S., Douville, J., et al. (2024). Antisense oligonucleotide therapy in an individual with KIF1A-associated neurological disorder. Nat. Med. *30*, 2782–2786. https://doi.org/10.1038/s41591-024-03197-y.

37. Lentz, J.J., Pan, B., Ponnath, A., Tran, C.M., Nist-Lund, C., Galvin, A., Goldberg, H., Robillard, K.N., Jodelka, F.M., Farris, H.E., et al. (2020). Direct Delivery of Antisense Oligonucleotides to the Middle and Inner Ear Improves Hearing and Balance in Usher Mice. Mol. Ther. *28*, 2662–2676. https://doi.org/10.1016/j.ymthe.2020.08.002.

38. Lentz, J.J., Jodelka, F.M., Hinrich, A.J., McCaffrey, K.E., Farris, H.E., Spalitta, M.J., Bazan, N.G., Duelli, D.M., Rigo, F., and Hastings, M.L. (2013). Rescue of hearing and vestibular function by antisense oligonucleotides in a mouse model of human deafness. Nat. Med. *19*, 345–350. https://doi.org/10.1038/nm.3106.

39. Skotte, N.H., Southwell, A.L., Østergaard, M.E., Carroll, J.B., Warby, S.C., Doty, C. N., Petoukhov, E., Vaid, K., Kordasiewicz, H., Watt, A.T., et al. (2014). Allele-Specific Suppression of Mutant Huntingtin Using Antisense Oligonucleotides: Providing a Therapeutic Option for All Huntington Disease Patients. PLOS ONE *9*, e107434. https://doi.org/10.1371/journal.pone.0107434.

40. Østergaard, M.E., Southwell, A.L., Kordasiewicz, H., Watt, A.T., Skotte, N.H., Doty, C.N., Vaid, K., Villanueva, E.B., Swayze, E.E., Bennett, C.F., et al. (2013). Rational design of antisense oligonucleotides targeting single nucleotide polymorphisms for potent and allele selective suppression of mutant Huntingtin in the CNS. Nucleic Acids Res. *41*, 9634–9650. https://doi.org/10.1093/nar/gkt725.

41. Rinaldi, C., and Wood, M.J.A. (2018). Antisense oligonucleotides: the next frontier for treatment of neurological disorders. Nat. Rev. Neurol. *14*, 9–21. https://doi.org/10.1038/nrneurol.2017.148.

42. Shen, W., De Hoyos, C.L., Migawa, M.T., Vickers, T.A., Sun, H., Low, A., Bell, T.A., Riney, S., Murray, S.F., Greenlee, S., and Crooke, R.M. (2019). Chemical modification of PS-ASO therapeutics reduces cellular protein-binding and improves the therapeutic index. Nat. Biotechnol. *37*, 640–650. https://doi.org/10.1038/s41587-019-0106-2.

43. Benson, M.D., Waddington-Cruz, M., Berk, J.L., Polydefkis, M., Dyck, P.J., Wang, A. K., Planté-Bordeneuve, V., Barroso, F.A., Merlini, G., Obici, L., et al. (2018). Inotersen Treatment for Patients with Hereditary Transthyretin Amyloidosis. N. Engl. J. Med. *379*, 22–31. https://doi.org/10.1056/NEJMoa1716793.

44. Witztum, J.L., Gaudet, D., Freedman, S.D., Alexander, V.J., Digenio, A., Williams, K. R., Yang, Q., Hughes, S.G., Geary, R.S., Arca, M., et al. (2019). Volanesorsen and Triglyceride Levels in Familial Chylomicronemia Syndrome. N. Engl. J. Med. *381*, 531–542. https://doi.org/10.1056/NEJMoa1715944.

45. Rukov, J.L., Hagedorn, P.H., Høy, I.B., Feng, Y., Lindow, M., and Vinther, J. (2015). Dissecting the target specificity of RNase H recruiting oligonucleotides using massively parallel reporter analysis of short RNA motifs. Nucleic Acids Res. *43*, 8476–8487. https://doi.org/10.1093/nar/gkv759.

46. Finkel, R.S., Mercuri, E., Darras, B.T., Connolly, A.M., Kuntz, N.L., Kirschner, J., Chiriboga, C.A., Saito, K., Servais, L., Tizzano, E., et al. (2017). Nusinersen versus Sham Control in Infantile-Onset Spinal Muscular Atrophy. N. Engl. J. Med. *377*, 1723–1732. https://doi.org/10.1056/NEJMoa1702752.

47. Mathiesen, B.K., Miyakoshi, L.M., Cederroth, C.R., Tserga, E., Versteegh, C., Bork, P.A.R., Hauglund, N.L., Gomolka, R.S., Mori, Y., Edvall, N.K., et al. (2023). Delivery of gene therapy through a cerebrospinal fluid conduit to rescue hearing in adult mice. Sci. Transl. Med. *15*, eabq3916. https://doi.org/10.1126/scitranslmed.abq3916.

48. Beisel, K.W., Rocha-Sanchez, S.M., Morris, K.A., Nie, L., Feng, F., Kachar, B., Yamoah, E.N., and Fritzsch, B. (2005). Differential expression of KCNQ4 in inner hair cells and sensory neurons is the basis of progressive high-frequency hearing loss. J. Neurosci. *25*, 9285–9293. https://doi.org/10.1523/jneurosci.2110-05.2005.

49. Pardridge, W.M. (2016). CSF, blood-brain barrier, and brain drug delivery. Expert Opin. Drug Deliv. *13*, 963–975. https://doi.org/10.1517/17425247.2016.1171315.

50. Sakka, L., Coll, G., and Chazal, J. (2011). Anatomy and physiology of cerebrospinal fluid. Eur. Ann. Otorhinolaryngol. Head Neck Dis. *128*, 309–316. https://doi.org/10.1016/j.anorl.2011.03.002.

51. Spector, R., Robert Snodgrass, S., and Johanson, C.E. (2015). A balanced view of the cerebrospinal fluid composition and functions: Focus on adult humans. Exp. Neurol. *273*, 57–68. https://doi.org/10.1016/j.expneurol.2015.07.027.

52. Cui, C., Wang, D., Huang, B., Wang, F., Chen, Y., Lv, J., Zhang, L., Han, L., Liu, D., Chen, Z.Y., et al. (2022). Precise detection of CRISPR-Cas9 editing in hair cells in the treatment of autosomal dominant hearing loss. Mol. Ther. Nucleic Acids *29*, 400–412. https://doi.org/10.1016/j.omtn.2022.07.016.

53. Zhang, X., Shi, T., Li, J., Wu, X., Wu, K., Li, D., Wang, D., Guan, J., and Wang, H. (2024). Natural History of KCNQ4 p.G285S Related Hearing Loss, Construction of iPSC and Mouse Model. Laryngoscope *134*, 2356–2363. https://doi.org/10.1002/lary.31179.

54. Mammano, F., and Ashmore, J.F. (1996). Differential expression of outer hair cell potassium currents in the isolated cochlea of the guinea-pig. J. Physiol. *496* (Pt 3), 639–646. https://doi.org/10.1113/jphysiol.1996.sp021715.

55. Leitner, M.G., Feuer, A., Ebers, O., Schreiber, D.N., Halaszovich, C.R., and Oliver, D. (2012). Restoration of ion channel function in deafness-causing KCNQ4 mutants by synthetic channel openers. Br. J. Pharmacol. *165*, 2244–2259. https://doi.org/10.1111/j.1476-5381.2011.01697.x.

56. Kirjavainen, A., Laos, M., Anttonen, T., and Pirvola, U. (2015). The Rho GTPase Cdc42 regulates hair cell planar polarity and cellular patterning in the developing cochlea. Biol. Open *4*, 516–526. https://doi.org/10.1242/bio.20149753.

57. Bai, J.P., Surguchev, A., Ogando, Y., Song, L., Bian, S., Santos-Sacchi, J., and Navaratnam, D. (2010). Prestin surface expression and activity are augmented by interaction with MAP1S, a microtubule-associated protein. J. Biol. Chem. *285*, 20834–20843. https://doi.org/10.1074/jbc.M110.117853.
58. Toonen, L.J.A., Casaca-Carreira, J., Pellisé-Tintoré, M., Mei, H., Temel, Y., Jahanshahi, A., and van Roon-Mom, W.M.C. (2018). Intracerebroventricular Administration of a 2'-O-Methyl Phosphorothioate Antisense Oligonucleotide Results in Activation of the Innate Immune System in Mouse Brain. Nucleic Acid Ther. *28*, 63–73. https://doi.org/10.1089/nat.2017.0705.
59. Pollak, A.J., Zhao, L., Vickers, T.A., Huggins, I.J., Liang, X.H., and Crooke, S.T. (2022). Insights into innate immune activation via PS-ASO-protein-TLR9 interactions. Nucleic Acids Res. *50*, 8107–8126. https://doi.org/10.1093/nar/gkac618.
60. Moazami, M.P., Rembetsy-Brown, J.M., Sarli, S.L., McEachern, H.R., Wang, F., Ohara, M., Wagh, A., Kelly, K., Krishnamurthy, P.M., Weiss, A., et al. (2024). Quantifying and mitigating motor phenotypes induced by antisense oligonucleotides in the central nervous system. Mol. Ther. *32*, 4401–4417. https://doi.org/10.1016/j.ymthe.2024.10.024.
61. Iwamoto, N., Butler, D.C.D., Svrzikapa, N., Mohapatra, S., Zlatev, I., Sah, D.W.Y., Standley, S.M., Standley, S.M., Lu, G., Apponi, L.H., et al. (2017). Control of phosphorothioate stereochemistry substantially increases the efficacy of antisense oligonucleotides. Nat. Biotechnol. *35*, 845–851. https://doi.org/10.1038/nbt.3948.
62. Tran, H., Moazami, M.P., Yang, H., McKenna-Yasek, D., Douthwright, C.L., Pinto, C., Metterville, J., Shin, M., Sanil, N., Dooley, C., et al. (2022). Suppression of mutant C9orf72 expression by a potent mixed backbone antisense oligonucleotide. Nat. Med. *28*, 117–124. https://doi.org/10.1038/s41591-021-01557-6.
63. Akita, J., Abe, S., Shinkawa, H., Kimberling, W.J., and Usami, S. (2001). Clinical and genetic features of nonsyndromic autosomal dominant sensorineural hearing loss: KCNQ4 is a gene responsible in Japanese. J. Hum. Genet. *46*, 355–361. https://doi.org/10.1007/s100380170053.
64. Topsakal, V., Pennings, R.J.E., te Brinke, H., Hamel, B., Huygen, P.L.M., Kremer, H., and Cremers, C.W.R.J. (2005). Phenotype determination guides swift genotyping of a DFNA2/KCNQ4 family with a hot spot mutation (W276S). Otol. Neurotol. *26*, 52–58. https://doi.org/10.1097/00129492-200501000-00009.
65. Chen, S., Francioli, L.C., Goodrich, J.K., Collins, R.L., Kanai, M., Wang, Q., Alföldi, J., Watts, N.A., Vittal, C., Gauthier, L.D., et al. (2024). A genomic mutational constraint map using variation in 76,156 human genomes. Nature *625*, 92–100. https://doi.org/10.1038/s41586-023-06045-0.
66. Cheerie, D., Meserve, M.M., Beijer, D., Kaiwar, C., Newton, L., Taylor Tavares, A.L., Verran, A.S., Sherrill, E., Leonard, S., Sanders, S.J., et al. (2025). Consensus guidelines for assessing eligibility of pathogenic DNA variants for antisense oligonucleotide treatments. Am. J. Hum. Genet. *112*, 975–983. https://doi.org/10.1016/j.ajhg.2025.02.017.
67. Ma, F., Yang, L., Sun, Z., Chen, J., Rui, X., Glass, Z., and Xu, Q. (2020). Neurotransmitter-derived lipidoids (NT-lipidoids) for enhanced brain delivery through intravenous injection. Sci. Adv. *6*, eabb4429. https://doi.org/10.1126/sciadv.abb4429.
68. Vihma, H., Li, K., Welton-Arndt, A., Smith, A.L., Bettadapur, K.R., Gilmore, R.B., Gao, E., Cotney, J.L., Huang, H.C., Collins, J.L., et al. (2024). Ube3a unsilencer for the potential treatment of Angelman syndrome. Nat. Commun. *15*, 5558. https://doi.org/10.1038/s41467-024-49788-8.
69. Gee, H.Y., Tang, B.L., Kim, K.H., and Lee, M.G. (2010). Syntaxin 16 binds to cystic fibrosis transmembrane conductance regulator and regulates its membrane trafficking in epithelial cells. J. Biol. Chem. *285*, 35519–35527. https://doi.org/10.1074/jbc.M110.162438.
70. Li, H., and Durbin, R. (2009). Fast and accurate short read alignment with Burrows-Wheeler transform. Bioinformatics *25*, 1754–1760. https://doi.org/10.1093/bioinformatics/btp324.
71. Bong, D., Sohn, J., and Lee, S.-J.V. (2024). Brief guide to RT-qPCR. Mol. Cells *47*, 100141. https://doi.org/10.1016/j.mocell.2024.100141.
72. Kechin, A., Boyarskikh, U., Kel, A., and Filipenko, M. (2017). cutPrimers: A New Tool for Accurate Cutting of Primers from Reads of Targeted Next Generation Sequencing. J. Comput. Biol. *24*, 1138–1143. https://doi.org/10.1089/cmb.2017.0096.
73. Callahan, B.J., McMurdie, P.J., Rosen, M.J., Han, A.W., Johnson, A.J.A., and Holmes, S.P. (2016). DADA2: High-resolution sample inference from Illumina amplicon data. Nat. Methods *13*, 581–583. https://doi.org/10.1038/nmeth.3869.
74. Lee, G.-Y., Ham, S., and Lee, S.-J.V. (2024). Brief guide to RNA sequencing analysis for nonexperts in bioinformatics. Mol. Cells *47*, 100060. https://doi.org/10.1016/j.mocell.2024.100060.
75. Bolger, A.M., Lohse, M., and Usadel, B. (2014). Trimmomatic: a flexible trimmer for Illumina sequence data. Bioinformatics *30*, 2114–2120. https://doi.org/10.1093/bioinformatics/btu170.
76. Pertea, M., Kim, D., Pertea, G.M., Leek, J.T., and Salzberg, S.L. (2016). Transcript-level expression analysis of RNA-seq experiments with HISAT, StringTie and Ballgown. Nat. Protoc. *11*, 1650–1667. https://doi.org/10.1038/nprot.2016.095.
77. Liao, Y., Smyth, G.K., and Shi, W. (2014). featureCounts: an efficient general purpose program for assigning sequence reads to genomic features. Bioinformatics *30*, 923–930. https://doi.org/10.1093/bioinformatics/btt656.
78. Love, M.I., Huber, W., and Anders, S. (2014). Moderated estimation of fold change and dispersion for RNA-seq data with DESeq2. Genome Biol. *15*, 550. https://doi.org/10.1186/s13059-014-0550-8.
79. Xu, S., Hu, E., Cai, Y., Xie, Z., Luo, X., Zhan, L., Tang, W., Wang, Q., Liu, B., Wang, R., et al. (2024). Using clusterProfiler to characterize multiomics data. Nat. Protoc. *19*, 3292–3320. https://doi.org/10.1038/s41596-024-01020-z.
80. Hänzelmann, S., Castelo, R., and Guinney, J. (2013). GSVA: gene set variation analysis for microarray and RNA-seq data. BMC Bioinformatics *14*, 7. https://doi.org/10.1186/1471-2105-14-7.
81. Sun, G., Zheng, Y., Fu, X., Zhang, W., Ren, J., Ma, S., Sun, S., He, X., Wang, Q., Ji, Z., et al. (2023). Single-cell transcriptomic atlas of mouse cochlear aging. Protein Cell *14*, 180–201. https://doi.org/10.1093/procel/pwac058.
82. Yu, R.Z., Baker, B., Chappell, A., Geary, R.S., Cheung, E., and Levin, A.A. (2002). Development of an ultrasensitive noncompetitive hybridization-ligation enzyme-linked immunosorbent assay for the determination of phosphorothioate oligodeoxynucleotide in plasma. Anal. Biochem. *304*, 19–25. https://doi.org/10.1006/abio.2002.5576.
83. Wei, X., Dai, G., Marcucci, G., Liu, Z., Hoyt, D., Blum, W., and Chan, K.K. (2006). A specific picomolar hybridization-based ELISA assay for the determination of phosphorothioate oligonucleotides in plasma and cellular matrices. Pharm. Res. *23*, 1251–1264. https://doi.org/10.1007/s11095-006-0082-3.
84. Jung, J., Joo, S.Y., Min, H., Roh, J.W., Kim, K.A., Ma, J.H., Rim, J.H., Kim, J.A., Kim, S.J., Jang, S.H., et al. (2024). MYH1 deficiency disrupts outer hair cell electromotility, resulting in hearing loss. Exp. Mol. Med. *56*, 2423–2435. https://doi.org/10.1038/s12276-024-01338-4.
85. Roh, J.W., Gee, H.Y., Wainger, B., Kim, W.K., Lee, W., and Nam, J.H. (2024). Distinct modulation of calcium-activated chloride channel TMEM16A by drug-binding sites. Proc. Natl. Acad. Sci. USA *121*, e2314011121. https://doi.org/10.1073/pnas.2314011121.
86. Altoe, A., Pulkki, V., and Verhulst, S. (2018). The effects of the activation of the inner-hair-cell basolateral K(+) channels on auditory nerve responses. Hear Res. *364*, 68–80. https://doi.org/10.1016/j.heares.2018.03.029.
87. Dierich, M., Altoè, A., Koppelmann, J., Evers, S., Renigunta, V., Schäfer, M.K., Naumann, R., Verhulst, S., Oliver, D., and Leitner, M.G. (2020). Optimized Tuning of Auditory Inner Hair Cells to Encode Complex Sound through Synergistic Activity of Six Independent K(+) Current Entities. Cell Rep. *32*, 107869. https://doi.org/10.1016/j.celrep.2020.107869.
88. Virtanen, P., Gommers, R., Oliphant, T.E., Haberland, M., Reddy, T., Cournapeau, D., Burovski, E., Peterson, P., Weckesser, W., Bright, J., et al. (2020). SciPy 1.0: fundamental algorithms for scientific computing in Python. Nat. Methods *17*, 261–272. https://doi.org/10.1038/s41592-019-0686-2.
89. Harris, C.R., Millman, K.J., van der Walt, S.J., Gommers, R., Virtanen, P., Cournapeau, D., Wieser, E., Taylor, J., Berg, S., Smith, N.J., et al. (2020). Array programming with NumPy. Nature *585*, 357–362. https://doi.org/10.1038/s41586-020-2649-2.